T.R.

GEBZE TECHNICAL UNIVERSITY

GRADUATE SCHOOL OF NATURAL AND APPLIED SCIENCES

THE STUDY OF HEAT TREATMENT PROCESS PARAMETERS IN Ni-BASED SINGLE CRYSTAL CMSX-4 SUPERALLOYS

GÖKHAN GÜNAY

A THESIS SUBMITTED FOR THE DEGREE OF

MASTER OF SCIENCE

DEPARTMENT OF MATERIALS SCIENCE AND ENGINEERING

GEBZE

2017

T.R.

GEBZE TECHNICAL UNIVERSITY

GRADUATE SCHOOL OF NATURAL AND APPLIED SCIENCES

THE STUDY OF HEAT TREATMENT PROCESS PARAMETERS IN Ni-BASED SINGLE CRYSTAL CMSX-4 SUPERALLOYS

GÖKHAN GÜNAY

A THESIS SUBMITTED FOR THE DEGREE OF

MASTER OF SCIENCE

DEPARTMENT OF MATERIALS SCIENCE AND ENGINEERING

THESIS SUPERVISOR

PROF. DR. METİN USTA

II. THESIS SUPERVISOR

DR. HÜSEYİN AYDIN

GEBZE

2017

T.C.
GEBZE TEKNİK ÜNİVERSİTESİ
FEN BİLİMLERİ ENSTİTÜSÜ

NİKEL ESASLI TEK KRİSTAL CMSX-4 SÜPERALAŞIMLARIN ISIL İŞLEM PROSES PARAMETRELERİNİN İNCELENMESİ

GÖKHAN GÜNAY
YÜKSEK LİSANS TEZİ
MALZEME BİLİMİ VE MÜHENDİSLİĞİ ANABİLİM DALI

DANIŞMANI
PROF. DR. METİN USTA
II. DANIŞMANI
DR. HÜSEYİN AYDIN

GEBZE
2017

GEBZE TEKNİK ÜNİVERSİTESİ	**YÜKSEK LİSANS JÜRİ ONAY FORMU**

GTÜ Fen Bilimleri Enstitüsü Yönetim Kurulu'nun 07/06/2017 tarih ve 2017/30 sayılı kararıyla oluşturulan jüri tarafından 21/06/2017 tarihinde tez savunma sınavı yapılan Gökhan Günay'ın tez çalışması Malzeme Bilimi ve Mühendisliği Anabilim Dalında YÜKSEK LİSANS tezi olarak kabul edilmiştir.

JÜRİ

ÜYE (TEZ DANIŞMANI)	: Prof. Dr. Metin USTA
ÜYE	: Prof. Dr. Fevzi BEDİR
ÜYE	: Yrd. Doç. Dr. Işıl KUTBAY

ONAY

Gebze Teknik Üniversitesi Fen Bilimleri Enstitüsü Yönetim Kurulu'nun ...../...../..... tarih ve ...../..... sayılı kararı.

İMZA/MÜHÜR

Doç. Dr. Arif Çağdaş AYDINOĞLU
Gebze Teknik Üniversitesi
Fen Bilimleri Enstitüsü Müdürü

SUMMARY

Single crystal (SX) superalloys are widely used in the core engine parts of aircraft turbofan engines. Generically, CMSX-4 alloys are the most common SX alloys used in these turbofan engine blades due to their high temperature mechanical properties and thermal oxidation resistance.

In these alloys, various refractory and rare earth elements which have low diffusion rates are used as an alloying element to enhance mechanical properties, corrosion resistance and creep properties. Hence, heat treatment processes are more complex and take more time than the usual heat treatment processes for other high-temperature alloys.

In this thesis, the heat treatment process parameters for CMSX-4 high-temperature superalloys are subsequently determined by several processes, microstructural analysis, and mechanical tests. Two heat treatment processes are performed to observe the effects of eutectic regions in CMSX-4 superalloys. The eutectic regions are completely dissolved after the standard heat treatment (SHT) process, while these eutectic regions remain as undissolved after the modified heat treatment (MHT) process. The morphological and mechanical properties of CMSX-4 are determined for each heat treatment process applied to the specimens. SHT process, it is determined that the eutectic regions are completely dissolved after SHT process while undissolved γ/γ' eutectics are observed in MHT specimens. After the heat treatment processes, γ and γ' precipitates are distributed at the appropriate size.

After mechanical tests, it is determined that the MHT specimens show higher resistance at room temperature. The tests at 982°C showed higher strength compared to the tests applied at 1038 °C. No significant difference is observed in terms of yield strengths of both heat-treated specimens at 982 °C. In comparison to the tensile test results, SHT specimens show higher strength in stress rupture tests than the MHT specimens. No significant difference is observed on hardness of specimens and the eutectic regions.

Key Words: Ni-based SX superalloys, CMSX-4, heat treatment, mechanical properties.

ÖZET

Tek kristal (SX) süperalaşımlar havacılıkta kullanılan türbinli motorların parçalarında yaygın olarak kullanılmaktadır. Genellikle, CMSX-4 alaşımları, yüksek sıcaklıkta gösterdikleri mekanik özellikleri ve iyi ısıl oksitlenme direnci nedeniyle turbofan motor kanatlarında en yaygın kullanılan SX alaşımlardır.

Bu alaşımlarda düşük difüzyon hızlarına sahip çeşitli refrakter ve nadir toprak elementleri; daha iyi mekanik özellik, korozyon direnci ve sürünme özelliklerini geliştirmek amacıyla alaşım elementi olarak kullanılırlar. Bu nedenle, bu alaşımların ısıl işlem prosedürleri daha karmaşık olup, diğer yüksek sıcaklık alaşımlara uygulanan ısıl işlem proseslerine göre daha uzun sürmektedir.

Bu tez çalışmasında, CMSX-4 yüksek sıcaklık süperalaşımların ısıl işlem proses parametreleri uygun ısıl işlem sıcaklık aralığı göz önüne alınarak çeşitli prosesler uygulanarak, mikro-yapısal analiz ve mekanik testlerle belirlenmiştir. Bu çalışmada, CMSX-4 süperalaşımına iki farklı ısıl işlem prosesi uygulanmıştır ve bu ısıl işlemlerin numune üzerinde gösterdiği morfolojik ve mekanik etkileri belirlenmiştir. Uygulanan standart ısıl işlem sonrası ötektik bölgelerin tamamen çözündüğü tespit edilmiş olup, uyarlanan ısıl işlem sonrasında ötektik fazların varlığı gözlenmiştir. Bu ısıl işlemler sonrasında γ ve γ' çözeltilerinin uygun boyutta dağılım gösterdiği belirlenmiştir.

Yapılan mekanik testler sonucunda, oda sıcaklığı için uyarlanmış ısıl işlem uygulanmış malzemenin daha iyi dayanım gösterdiği belirlenmiştir. 982 °C sıcaklıkta yapılan testlerde numuneler, 1038 °C'de yapılan testlere nazaran daha düşük uzama göstermesine karşılık, daha yüksek dayanım gösterdiği belirlenmiştir. Gerilim-kopma test sonuçlarında standart ısıl işlem uygulanmış numunelerden daha iyi dayanım verileri elde edilmiştir.

Sertlik deneyleri sonucunda, iki ısıl işlem uygulanmış numuneler arasında önemli bir farklılık gözlenmemiştir fakat standart ısıl işlem uygulanmış numunelerde daha iyi bir sertlik verileri elde edilmiştir. Uyarlanmış ısıl işlem sonrası yapıda bulunan ötektik bölgelerden alınan sonuçlar ile döküm hali numunelerinin ötektik bölgelerinden alınan sertlik değerleri arasında önemli bir farklılık gözlenmemiştir.

Anahtar kelimeler: Ni-esaslı SX süperalaşımlar, CMSX-4, ısıl işlem, mekanik özellikler.

ACKNOWLEDGEMENTS

I would like to express my gratitude to my supervisor Prof. Dr. Metin USTA for his permanent encouragement, supervision, and guidance during this thesis. I have been extremely lucky to have a supervisor who cared so much about my work, and who responded to my questions and queries so promptly.

With his effort and guidance, I also would like to express my gratitude to my co-supervisor, Dr. Hüseyin AYDIN. He always supported and guided me with his creative ideas on this long journey. Without his knowledge, experience and inquiring mind, this thesis might not proceed that much.

I am so much thankful to Assoc. Prof. Dr. Havva Kazdal ZEYTİN whom showed me the way I have to follow and helped me to find the answers when I was face up with.

I would like to express my sincere thanks to TÜBİTAK MRC Critical Metallic Materials Group members for their dynamic support and help in every step of this thesis. I also must thank especially to Erdem GÜNGÖR for his valuable supports.

I would like to express my sincere thanks to Ahmet NAZIM from Gebze Technical University for his help in EDS and SEM analysis. I also must thank to Assist. Prof. Dr. Işıl KUTBAY and Dr. Salim Levent AKTUĞ for their valuable supports during this thesis.

I must express my special thanks to my friends for their invaluable friendships and always being there for me.

Finally, the greatest gratitude is to my mother Hülya GÜNAY, to my father İskender GÜNAY, to my brother Mehmet GÜNAY and to my sister Dudu İzgi GÜNAY for their endless love, support, encouragement, patience and the opportunities they provided me in every step of my life. Thanks to them for always being beside me and hope they will always be.

This thesis was part of “5155A10- Development of Ni-based superalloys and production process used in aviation” project of TÜBİTAK MRC-Materials Institute, Critical Metallic Materials Group which is supported by “Undersecretariat for Defence Industries” of Turkey and Tusas Engine Industries Inc-TEİ (as contractor).

TABLE of CONTENTS

LIST of ABBREVIATIONS and ACRONYMS

Abbreviations and Acronyms		**Explanations**
AC	:	Air Cooling
BCC	:	Body Centered Cubic
CT	:	Computed Tomography
DS	:	Directional Solidification
DSC	:	Differential Scanning Calorimeter
DTA	:	Differential Thermal Analysis
EDS	:	Energy Dispersive X-ray Spectroscopy
FCC	:	Face Centered Cubic
FDD	:	Focus Detector Distance
FOD	:	Focus Object Distance
GFC	:	Gas Fan Cooling
GTU	:	Gebze Technical University
HT	:	High Temperature
OM	:	Optical Microscopy
LTE	:	Long Term Exposing
MHT	:	Modified Heat Treatment
PDAS	:	Primary Dendritic Arm Spacing
RT	:	Room Temperature
SDAS	:	Secondary Dendritic Arm Spacing
SEM	:	Scanning Electron Microscopy
SHT	:	Solution Heat Treatment
SR	:	Stress Rupture
SX	:	Single Crystal
TCP	:	Topological Close Packed
VIM	:	Vacuum Induction Melting
XRD	:	X-Ray Diffraction

LIST of FIGURES

LIST of TABLES

1. INTRODUCTION

Superalloys are known as the main alloys in aircraft engines with their enhanced properties at higher temperatures, higher stresses and under corrosive environments. Since the 1950s, superalloys are used on the aircraft engine turbine blades which require more than 5000h creep strength and good corrosion strength at high temperatures. Their properties vary depending on each part related to the engine and its operating temperature. As an example, combustion chambers goes up to the temperatures above 900°C and these components should resist significant amount of temperature, pressure and oxidation strength in these temperatures [1, 2].

Theoretically, all thermodynamic and kinetic parameters are taken to interest during the alloy selection of superalloys. In particularly, casting type, post process parameters and even coating environments should be controlled due to extreme conditions of the parts that operate in aerofoils.

The chemical composition is the key parameter for the structure-property relationship of superalloys. The influence of the elements in the composition determines the solidification parameters of the superalloy via primary dendrite spacing. With the presence of eutectic phases between dendrites, the mechanical properties of the superalloy changes throughout the material [3]. The nominal composition of Ni-based superalloys contain 10-20 % of Cr, 8% Ti – Al, 5-10 % Co and small amounts of Zr, C balanced with Ni. Some other elements like Mo, W, Ta, Hf can be added as an alloying element [4]. Al, Ti, Nb, Mo, W elements are added in order to obtain good mechanical strength and corrosion resistance. Table 1.1 shows some of the important Ni-based superalloys with an alphabetic order [5].

Nickel is tough and ductile due to its face centred cubic (FCC) crystal structure and owing to this, nickel is stable from room temperature to its melting temperature and not resulting with phase transformations, prevents expansion and shrinkage conditions, which restricts usage at high-temperature applications. Diffusion rate should be at lower rates in order to obtain lower creep rate. By the reason is that nickel has lower diffusion rates with its FCC structure, microstructural stability is substantially provided at higher temperatures. Ni-based superalloys are strengthened with solid-solutionized phases and secondary intermetallic phases via precipitation hardening. These intermetallic metals are by-products of Al, Ti, Nb [6, 7].

Table 1.1: The nominal compositions of some Ni-based superalloys.

Alloy	Cr	Co	Mo	W	Ta	Nb	Al	Ti	Fe	C	B	Zr	Re	Hf	Others
ATI 718Plus	19	9	2,8	1,1		5,6	1,45	0,75	9	0,03	0,006				
Astroloy	14,9	17,2	5,1				4	3,5		0,03		0,04			
CMSX2	8	4,6	0,6	7,9	5,8		5,6	0,9							
CMSX4	5,7	11	0,42	5,2	5,6		5,2	0,74					3	0,1	
CMSX6	9,8	5	3		2,1		4,8	4,7							
CMSX10	2	3	0,4	5	8	0,1	5,7	0,2					6	0,03	
FT750DC	20			3,5			2,3	2,1	5	0,07	0,005				0.4 Si
Hastelloy X	22	1,5	9	6					18,5	0,1					0.5Mn, 0.5Si
Hastelloy S	15,5		14,5				0,2		1	0,02	0,009				0.02 La
Inconel 600	15,8								7,2	0,04					0.2Mn, 0.2 Si
Inconel 718	18,6		3,1			5	0,4	0,9	18,5	0,04					0.2Mn, 0.3Si
Inconel 625	22	0,1	9			3,5	0,1	0,2	3	0,01					
MA758	30			0,5			0,3			0,05					0.6 yttria
MA760	19,5			3,4			6		1,2	0,06					1.0 yttria
MA6000	15			3,9			4,5	2,3	1,5	0,06					1.1 yttria
MAR-M200	9	10		12		1	5	2		0,15	0,015	0,05			
Nimonic 80A	19,5	1,1					1,3	2,5			0,06				
Nimonic 105	14,5	20	5					1,2	4,5		0,2				
PM1000	20						0,3	0,5	3						0.6 yttria
Rene N5	7	8	2	5	7		6,2						3	0,2	
Rene N6	4,2	12,5	1,4	6	7,2		5,75						5	0,15	
Rene 41	19	11	10				1,5	3,1		0,09	0,05				
RR2000	10	15	3				0,05	4							1 V
RR3000	2,3	3,3	0,4	5,5	8,4		5,8	0,2					6,3	0,03	
UCSX1	2,3	6	1,5	7	8,4		5,8	0,2					6,3	0,03	2 Ru
UCSX8	2,3	6	3	6	8,4		5,8	0,2					6,3	0,03	6Ru
SRR99	8,5	5		9,5	2,8		5,5	2,2							
TMS 63	6,9		7,5		8,4		5,8	0							
TMS75	3	12	2	6	6								5	0,1	
TMS138	3	12	3	6	6								5	0,1	2Ru
TMS162	2,9	5,8	3,9	5,8	5,6		5,8						4,9	0,1	6Ru
Udimet 500	18	18,5	4				2,9	2,9		0,08	0,006	0,05			
Udimet 700	15	18,5	5,2				4,3	3,5		0,08	0,03				
Waspaloy	19,5	13,5	4,3				1,3	3		0,08	0,006	0,06			

Ni-based superalloys are better than stainless steels from the point of mechanical strength, especially over 650°C temperatures. Solid solution alloys like Inconel 600, Inconel 601 and RA333 are widely used in the components of heat treatment equipment and different kinds of furnace components. The reason of that is these alloys have high oxidation - corrosion resistance and high mechanical strength which provide the properties required for these industrial areas. Other applications of Ni-based superalloys are hydroelectric and nuclear power plants [6, 7].

CMSX-4 is a nickel based single crystal (SX) superalloy which consists of 3 % of Re as an alloying element and precipitate strengthening phase, γ′ with 70% volume fraction. Their enhanced properties make these alloys favoured in the core part of the turboshaft and turbofan engine turbine blades'. In general, these parts perform at the

first stage of turbine engine and are exposed to significant amount of temperature and pressures compared to other parts of the turbine engine [2, 8]. Hence, alloying, processing and coating parameters required extreme dedication during the production of CMSX-4 SX turbine blades.

In this thesis, the heat treatment process parameters of nickel based SX CMSX-4 superalloys are determined to improve high-temperature mechanical properties of these alloys via homogenization and controlled precipitation of microstructure. For this purpose, various heat treatment processes are applied to observe the effect of step wise heating and controlled quenching. Then, microstructural characterization of these samples is studied via optical and electron microscopy techniques. Mechanical characterization of these samples is started with room and high temperature tensile tests and completed with stress rupture tests.

2. LITERATURE REVIEW

2.1. Background of Ni Based Superalloys

The history of superalloys goes back to 1940s. The development of the turbine blade materials and their processes depends on the improvements of superalloys. Wrought superalloys started to use at turbine blade applications at late 1950s. Then, due to the improvements of casting under vacuum technologies and the quality of alloying during casting; casting superalloys were favoured in 1960s. Figure 2.1 shows the evolution of these superalloys by years [1].

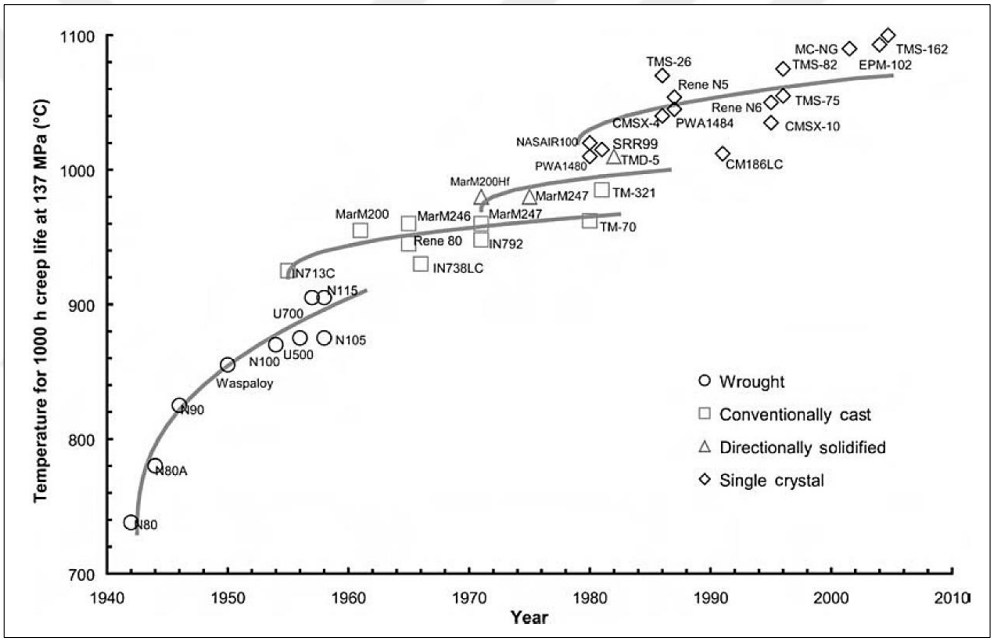

Figure 2.1: Evolution of the superalloys by years.

At 1970s, directionally solidification process was preferred as the main casting technique and used to obtain columnar structures which have no crosscut grain boundaries. Thus, the mechanical properties of the materials are improved. Figure 2.2 shows the grain growth mechanism based on types of turbine blades [1]. After the production of Ni based SX alloys started at late 1980s, the necessity of grain boundary strengthened elements B, C is reduced. Meanwhile, micro-segregation and the amount of eutectic phase were reduced by the improvement in heat treatment processes.

Modified heat treatments also prevented the local melting on the surface. Thus, the fatigue life was prolonged [1].

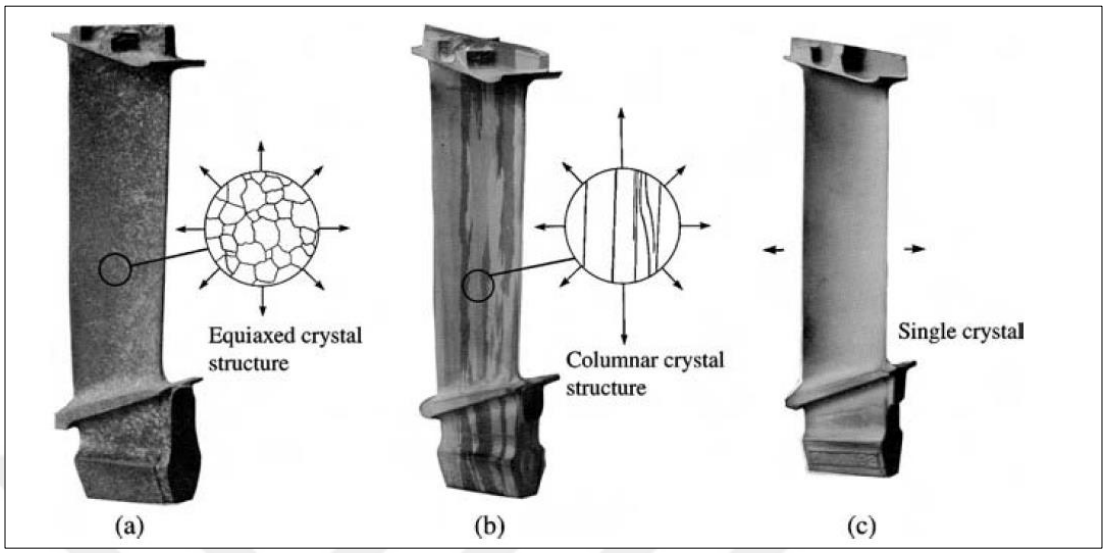

Figure 2.2: Turbine blades based on their crystal structures a) equiaxed, b) columnar and c) single-crystal forms.

SX superalloys had become widespread at mid-1990s in order to achieve best creep performances in gas turbine engines. For example, 1st generation SX superalloys like SRR99, under 850°C/250 MPa conditions, have 250h creep rupture life as well as for the 3rd generation SX superalloys like RR3000 creep rupture life is almost 2500h. Under the tough conditions as 1050°C/150MPa, creep-rupture strength increases from 250h to 1000h. Commercially used Ni-based SX superalloys and their compositions are shown in Table 2.1 [1, 9].

Table 2.1: Commercially used Ni-based SX superalloys.

Alloy	Cr	Co	Mo	W	Ta	Re	Ru	Nb	Al	Ti	Zr	B	C	Hf
PWA 1480	10	6		4	12				5	1.5				
Rene N4	12.8	9	1.9	3.8	4			0.5	3.7	4.2				
SRR99	8	5	0	10	3				5.5	2.2				
AM1	8	6	2	6	9				5.2	1.2				
AM3	8	6	2	5	4				6	2				
CMSX-2	8	5	0.6	8	6				5.6	1				
CMSX-3	8	5	0.6	8	6				5.6	1				0.1
CMSX-6	10	5	3	0	2				4.8	4.7				0.1
MC2	8	5	2	8	6				5	1.5				
CMSX-4	6.5	9	0.6	6	6.5	3			5.6	1	1			0.1
PWA 1484	6	10	2	6	9	3			5.6	0				0.1
SC180	5	10	2	5	8.5	3			5.2	1				0.1
LEK94	5.8-6.4	7.2-7.8	1.7-2.3	3-7	2-2.6	2.3-2.6			6.2-6.8	0.9-1.1				0.05-0.15
ReneN5	7	7.5	1.5	5	6.5	3			6.2	0			0.05	0.15
CMSX10	2	2	0.4	5	8	6		0.1	5.7	0.2				0.03
ReneN6	4.2	12.5	1.4	6	7.2	5.4		0.1	5.7	0		0.05		0.15
RR2100	2.5	12	0	9	5.5	6.4			6	0				0
TMS75	3	12	2	6	6	5			6	0				0.1
MCNG	4	0	1	5	5	4	4		5.2	1.1				0
EPMI02	2	16.5	2	6	8.25	5.95	3		5.55	0				0.15
RR2101	2.5	12	0	9	5.5	6.4	2		6	0				0
TMS173	2.8	5.6	2.8	5.6	5.6	6.9	5		5.6	0				0.1
TMS162	2.9	5.8	3.9	5.8	5.6	4.9	6		5.8	0				0.1
TMS196	4.6	5.6	2.4	5	5.6	6.4	5		5.8					0.1
TMS238	4.6	6.5	1.1	4	7.6	6.4	5		5.9	0				0.1

As can be seen in Table 2.1, 1st generation SX superalloys like PWA1480, Rene N4 and SRR99 alloys contain γ' phase strengthening elements Al, Ti, Ta. Grain boundary strengthening elements B and C are not used for SX superalloys [7]. 2nd generation SX superalloys like PWA1484, CMSX-4, Rene N5 and 3rd generation SX superalloys like CMSX-10, Rene N6 comprise 3%wt and 6%wt Re, respectively. In general, the compositions of new generation superalloys include low concentrations of Cr and high concentrations of Al, Re [1].

After 2000s, 4th generation SX superalloys like MC-NG, EPM-102 and TMS-162 were improved with 2-3%wt Ru additions [1]. In this case, Ru was used to prevent precipitating of TCP phases and improved the high temperature stability of microstructure. From the viewpoint of high temperature creep performances, 4th generation SX superalloys operates 30°C above the previous generation [10, 11].

The development of new generations is still an active scientific topic for the materials engineers; tough 5-6%wt Ru element is a levelling point for 5th generation SX superalloys. Lattice misfit of γ and γ' phases in these superalloys are controlled in order to balance strength and coherence of interface. 5th generation superalloys have thinner dislocation network between the interfaces of γ and γ' phases, in order to prevent dislocation movement under stress [10, 11].

2.1.1. Production of Superalloys

The investment casting process is the primary process used to produce difficult to machine superalloy parts with its complex ceramic mould design advantageous. This is why investment casting of superalloys is concerned with the manufacture of blades and vanes in turbine industry.

Firstly, the designated moulds and cores are produced with wax-bunch models in order to fabricate the ceramic moulds. The wax-bunch model is later immersed into the slurry which consists of different ceramic powders and left to dry in an autoclave furnace. During the autoclave process, the wax is removed from the shell mould via heating. After that, the ceramic shells are transferred to the conventional vacuum casting process.

In order to produce wrought or cast alloys, Vacuum Induction Melting (VIM) method is used as a first melting step and is a must to add high atmospheric oxygen and nitrogen rated elements to superalloys. VIM method is preferred in order to take all the low melting temperature impurities (non-metal residuals/contaminations) out of the system via vacuum. VIM method is favoured due to the existence of Al, Ti solutes in the compositions of Ni-based superalloys [12]. Figure 2.3 shows melting under vacuum and solidification system for Ni-based SX superalloys [13].

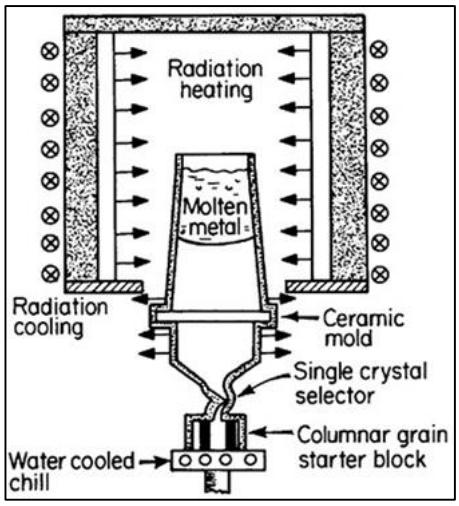

Figure 2.3: The system of melting under vacuum and solidification of Ni- based SX superalloys.

The conventional casting microstructure will be coaxial. When the columnar SX castings are produced at a controlled speed from a hot zone to a cold zone in furnace, the coaxial castings are obtained as a result of the solidification of the castings being fairly uniform throughout their volume. Following the initial solidification, the alloy is subjected to a series of heat treatment processes aimed at reducing segregation, producing a γ' precipitate phase, altering the grain boundary phases (especially carbides) and/or helping the coating process [14].

In each casting operation, the final structure of the material and therefore its properties are sensitive to the thermal conditions present during solidification. Solidification has dendritic character and the primary and / or secondary dendrite arm spacing is dependent on the G*R cooling rate. Figure 2.4 shows the change in dendrite morphology and the cooling rate (G * R) of the primary dendritic arm spacing (PDAS) during solidification [14]. The segregation tendency of alloying elements with dendritic solidification morphology is directly related to each other [14].

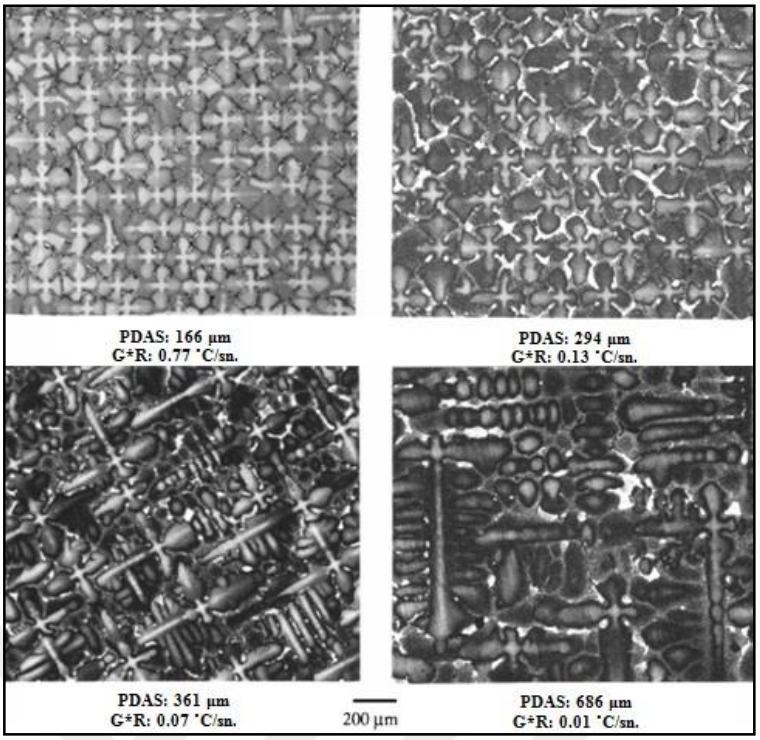

Figure 2.4: Changes in dendrite morphology and primary dendrite arm spacing (PDAS) with cooling rate (G*R) during solidification.

Nickel-based superalloys require a critical draw rate for producing SX castings. This value and the casting method are important to determine preform of solidification while temperature gradient and the cooling rate for determining the as-cast microstructure. An increase in the cooling rate reduces the distance between the primary and secondary dendrite arm spaces; and thus, it means decomposition of γ/γ′ eutectic and γ′ phases and consequently reduced dendritic microsegregation as well as time and cost of heat treatment process are obtained. The temperature gradient and chemical composition of the alloy affect the type and amount of defects (freckle defects, elongated grains, high and low angle boundaries) especially in large size castings [15].

2.1.2. Effect of Alloying Elements

The important properties of superalloys are determined by the elements in its content. These elements have different characteristic features and they have an important place in providing certain important properties. They change the lattice parameters of the γ and γ 'phases and therefore also change lattice misfit which effects mechanical properties. Superalloys can contain more than ten elements in their

content, mostly chromium (Cr), cobalt (Co), aluminum (Al). In addition, other alloying elements are added to provide different properties. These elements are some of the refractory elements like rhenium (Re), tungsten (W), tantalum (Ta), hafnium (Hf) from 5d block and some of elements like molybdenum (Mo), niobium (Nb), zirconium (Zr) etc. from the 4d block of the periodic table. Figure 2.5 shows the position and behaviour of the elements are located on the periodic table [1].

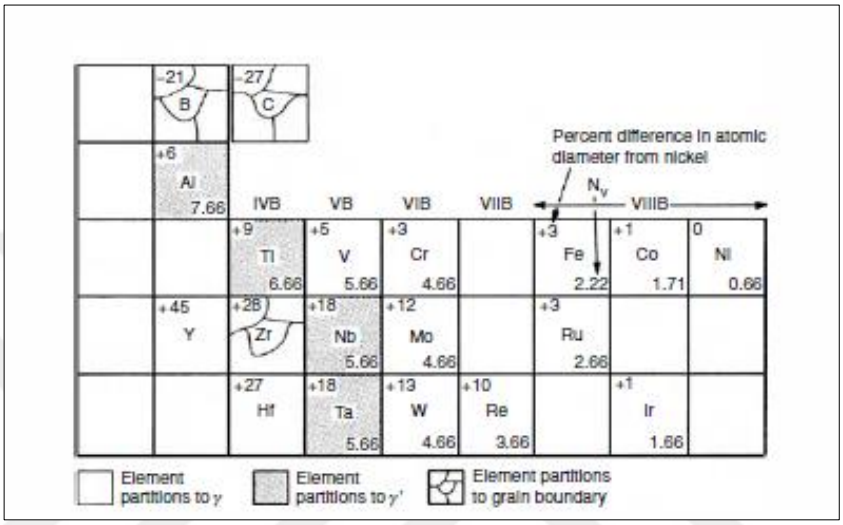

Figure 2.5: The elements used in Ni-based superalloys and their position at periodical table.

The elements such as Co, Mo, Re, W, whose atomic radius is close to Ni, dissolve and afterwards form the austenitic γ phase. Al, Ti, Ta have a larger atomic radius than Ni and play an important role in the formation of γ' phase via forming Ni_3(Al, Ta, Ti). The general effects of these elements are shown in Table 2.2 [1].

Table 2.2: The influences of the elements on Ni-based superalloys.

Effect	**Elements**
Solid solution strengtheners	Co, Cr, Mo, W, Ta, Re
Forms γ '	Al, Ti, Ta
Raises solvus temperature of γ '	Co
Hardening precipitates and/or intermetallics	Al, Ti, Nb
Oxidation Resistance	Al, Cr
Sulphidation Resistance	Cr, Co
Improves Creep Properties	Re, Ta
Retard γ ' Coarsening	Re

Re is an important element which classifies the generations of the superalloys in SX form. The first-generation alloys are not included with Re but after 2nd generation SX superalloys, at least 3% Re is included because of its role against especially creep performance. The additions of Re influence as an obstacle of coarsening of γ' particles and at the same time enabling γ' clusters to be stabilized depending on slow diffusivity of Re but however Re prevents microstructural homogeneity, while heat treatment process depending on low diffusivity of Re, and intensive microsegregation conditions. High ratio Re additions have a result of precipitating of topological close packed (TCP) phases and these precipitated phases negatively effect on creep properties in virtue of reducing strength improver elements from matrix, initiating fractures depending on stress concentration and preventing microstructural durability [10].

Re also effects on the hardness of γ phase positively but in spite of that some experiments show that Re has no effect on hardness of γ' phase [16]. Addition of Re element also increases the cost and the density.

In order to enhance high temperature performances of new generation Ni-based superalloys, the total percentage of refractory element additives are gradually increased. Nevertheless, additions of refractory elements like Re, W ends up with some problems such as excessive segregation formation, tendency to grain defects formation, more complex solution heat treatment processes and increasing harmful TCP phase formation.

The effective way to enhance the stress rupture strength of Ni-based superalloys over 1050˚C temperatures is decreasing percentage of Cr and increasing percentage of W. For instance, Cr is decreased about 2-4 % wt in third generation SX superalloys. Total percentage of refractory elements like W, Mo, Ta, Re is about 20% wt. Among these elements, Re has the positive effect on oxidation resistance, while Cr has opposite effect, and stress rupture strength [17].

In this thesis, Ni based SX superalloy CMSX-4 is used. The chemical composition of this alloy is shown in Table 2.3. The most important difference of CMSX-4 is 3% addition of Re in its content which is important for creep strength.

Table 2.3: The chemical composition of CMSX-4 in weight percent.

Cr	**Co**	**Mo**	**W**	**Ta**	**Re**	**Al**	**Ti**	**Hf**	**Ni**
6.5	**9.0**	**0.6**	**6.0**	**6.5**	**3.0**	**5.6**	**1.0**	**0.1**	**Ba**

2.2. CMSX-4

2.2.1. Importance of CMSX-4

Aviation industry made one of the most innovative step with the development of turbofan jet engines in 1980s. A turbofan jet engine consists of a compressor, combustion chamber, turbines and exhaust nozzle (Figure 2.6). In general, the blades in front of the turbofan engines are bigger than the blades inside. These blades work under 150℃, therefore, aluminium, titanium and stainless steels are favourable.

The next part of the turbofan engine is compressor. Blades boost the incoming air to the stator blades and the pressure goes up to 30 times more. So the temperature in this chamber increases to till 1000℃ level. Therefore, the materials used in here should have high strength values at high temperatures and should resist against fatigue, oxidation and creep. In this part, Ni-based superalloys are favourable due to their fascinating properties at higher temperatures. Ni-based superalloys are used over 800°C for the aircraft engines [1].

In the end part, the compressed air goes through combustor chamber and mixes with fuel and ignited. After this process, the temperature increases up to 1800℃ and therefore thermally barrier coated SX and directionally solidified (DS) Ni based superalloys become the material of choice. These superalloys comprise the elements like titanium, aluminium and also refractory metals (i.e. tungsten, molybdenum, niobium, tantalum and rhenium which has high resistance to high temperature, corrosion and wear) [18].

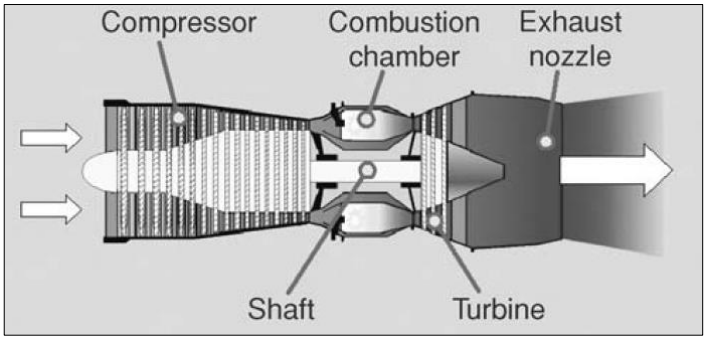

Figure 2.6: A simple illustration of a basic engine motor.

CMSX-4 is a 2nd generation Ni-based superalloy which is upgraded from 1st generation Ni-based superalloys in 1980s. In order to get enhanced properties, CMSX-4 improved with balancing Ta/W ratio, adding 3% Re, increasing Co content and reducing Cr ratio [19]. After addition of Re, creep strength and thermal fatigue resistance are improved in comparison to the 1st generation superalloys [19].

There are two main phases in CMSX-4 superalloys. These phases are "Gamma Phase (γ)" as matrix and "Gamma Prime Phase (γ')".

Gamma Phase is a nonmagnetic phase which has FCC crystal structure is that consisting high percent of some solid solution elements Co, Fe, Cr, Mo and W. All Ni-based superalloys have this phase as matrix [20].

Gamma Prime (γ') is another phase which is consisting after additions of Al, Ta and Ti metals for resisting to high temperatures and creep via constituting FCC structured, γ' (Ni_3Al,Ti) phase which is coherent to austenitic γ matrix. This phase is that forms $(Ni,Co)_3(Al,Ti)$ composition, is required for high-temperature strength and creep strength, and occurs which Al and Ti are settled dominantly inside [21-23]. Intermetallic γ', which is coherent to intermetallic γ-matrix, is formed via homogeneous nucleation process and spreads as fine form. These particles are firstly consisting antiphase boundary via dislocation intersects while deformation continuous, and then this antiphase boundary disappears after the second dislocation occurs (twin forms). A dislocation twin is separated by the diffusion controlling of antiphase boundary [22]. The strength improving the property of this phase is direct proportion to the temperature. γ' phase has the shape of a sphere or a cubic precipitate.

2.2.2. Single Crystal Casting Process

In SX casting process (schematically shown in Figure 2.3), the grains are placed in the lower part of the spiral grain selector which is shown in Figure 2.7 [24]. The grain at the top of the grain selector also fills the entire of the mould cavity [25].

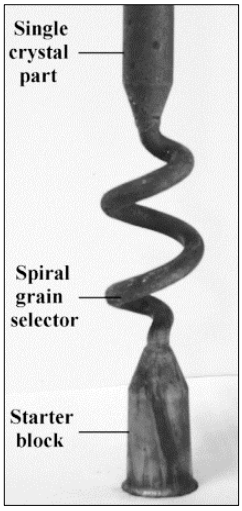

Figure 2.7: A typical grain selector used in SX solidification process**.**

The temperature gradient in the nucleation chamber is related to the cooling plate, molten metal and mould temperature. The mould temperature is generally about 1500-1600°C. On a water-cooled copper cooling plate, most grains nucleate randomly. As solidification continues, as can be seen in Figure 2.8, a few grains enter helix of grain selector [25]. Some grains are physically prevented from entering to the grain selector. After one or two turns, only one grain remains to growth [25].

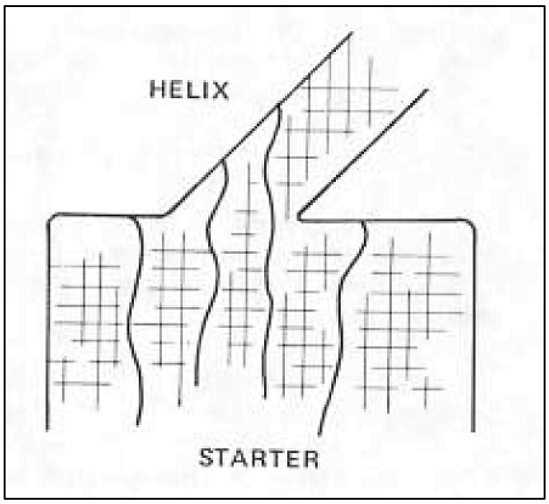

Figure 2.8: Schematically illustration of SX grain formation by grain selector.

The diameter of the spiral wire usually ranges from 0.3 to 0.5 cm, depending on the required heat flow and mould filling. A helix with a circular cross section is used to reduce grain nucleation in sharp edges. Changes in cross-sectional area occur during solidification process in a part. The grain nucleation at the cross-sectional area changes

can be avoided by appropriate flap design and heat flow control provided by the mould thickness [25].

The desired mechanical properties of the castings are obtained with the value of the angle of deviation α from [001] direction have to be less than 15°, if not, the creep performance of the material is going to be reduced [26].

2.3. Heat Treatment

CMSX-4 superalloys are subjected to a solution heat treatment process and a two-stage ageing heat treatment process.

2.3.1. Solution Heat Treatment Process

SX superalloys are subjected to solution heat treatment to obtain a suitable microstructure consisting of fine γ' precipitates free of eutectic phases and to homogenize microsegregation between dendrite and dendritic core [27]

In order to be able to apply appropriate heat treatments, the transition reactions of the material must be known. In particular, the size of the γ' precipitates and the gap between them are the important points. For Ni-based superalloys there must be a balance between the solidus temperature (the temperature at which the melting starts) and the solvus temperature (the temperature at which precipitating (γ' for CMSX-4) starts). Between these two temperatures are known as the heat treatment window. Heat treatment processes should be performed between these temperatures [28]. Figure 2.9 shows the heat treatment window schematically [28].

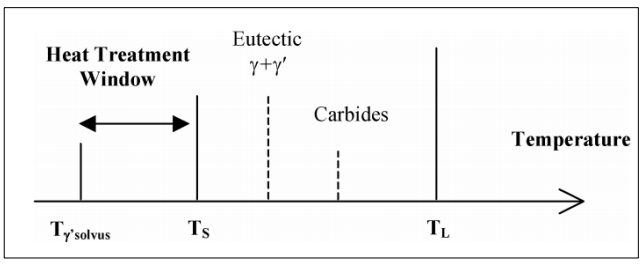

Figure 2.9: Schematic illustration of heat treatment window.

The temperature at the beginning of the first melting is important in order to determine the formation of these precipitates. Solvus temperature is also important to

control for an appropriate heat treatment process. A wider heat treatment window can be determined since a higher solvus temperature requires a higher melting incipient temperature [28].

Coarse γ' precipitates occur as a result of slow cooling during solidification following by casting process. Similarly, γ/γ' eutectic phases are formed in interdendritic regions during solidification. In order for SX superalloys to exhibit optimum mechanical properties, these phases must be homogenized by applying a suitable heat treatment process to the solution. To accomplish this, the alloy must be heated to the temperatures above the γ' solvus temperature, nevertheless but not over the melting point to avoid melting. This temperature range between the γ' solvus temperature and the melting temperature is called as heat treatment window. It is desirable that the heat treatment window is high for a successful solution heat treatment process [27, 29].

Despite the existing knowledge, the development of a suitable solution heat treatment for Ni-based superalloys is a problematic process. The first reason for this problem is that when analysed by differential scanning calorimeter (DSC), it is very difficult to distinguish the solvus and solidus curves because of the expansion of the corresponding endothermic and exothermic peaks due to chemical heterogeneity of the alloy. These phase transformation temperatures do not only change by heating and cooling rates, but also with the level of homogenization. The second reason is that it is quite difficult to completely dissolve coarse γ' precipitates with a low surface area by volume ratio in γ matrix. In high-segregated microstructure, the local solidus temperatures between the dendrites may be much lower than the average solvus temperatures. This leads to regional problems between the dendrites in the solution heat treatment process, which causes the dissolution process to be incomplete. In order to get over this regional melting problem, the solution heat treatment process is carried out step by step at different temperatures and durations. Each heat treatment step, which occurs with a certain increase in temperature and a certain time at the reached temperature, provides partial homogenization of the alloy and elimination of eutectic phases. Thus, the start of melting can be reduced to the earliest run. However, the step-by-step process of heat treatment at different temperatures and durations makes it difficult to control the process [30].

Figure 2.10 shows optical microscope images of the γ/γ' eutectic regions in the as-cast microstructure of the superalloy [31]. After solution heat treatment process,

many of γ/γ' eutectic regions dissolve in order to stabilize the microstructure. Duration of the solution heat treatment process is also important because existence of eutectic regions also provide positive effect on mechanical properties. Figure 2.11 shows optical micrographs of a superalloy after short term solution heat treatment process and long term solution heat treatment process, respectively [32]. Eutectic regions are completely dissolved after long term exposure to high temperatures.

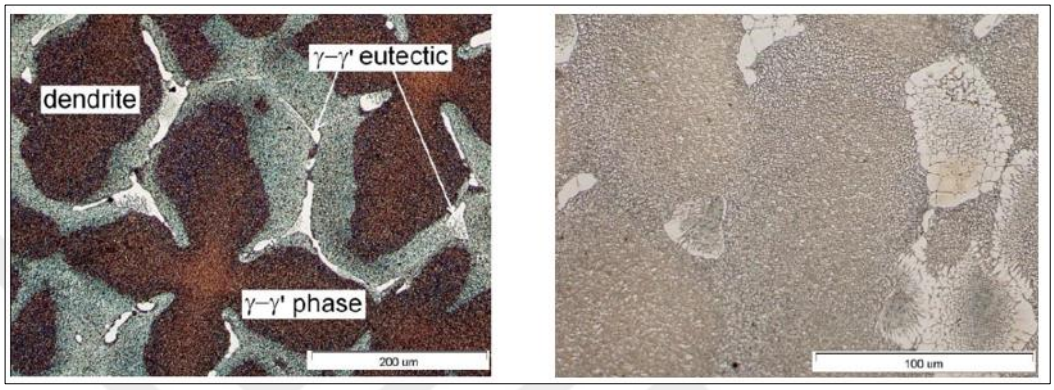

Figure 2.10: Optical microscope images of γ/γ' eutectic regions in as-cast microstructure of superalloy.

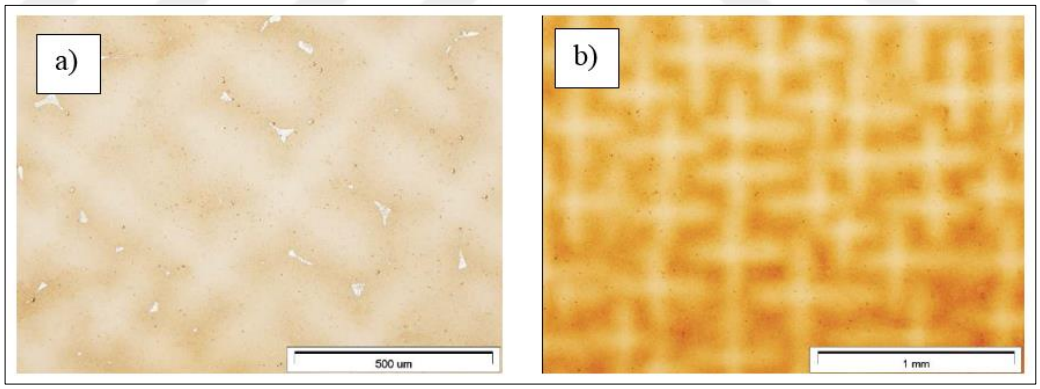

Figure 2.11: Optical microscope images of γ/γ' eutectic regions after a) short term solution heat treatment b) long term solution heat treatment.

Figure 2.12 shows the diffusion rate of the alloying elements in the nickel matrix depending on the temperature [27]. Figure 2.12 illustrates that the diffusion rate of rhenium (Re) and tungsten (W) elements in the nickel matrix is very slow. For this reason, the rhenium (Re) and tungsten (W), which are refractory elements, tend to segregate without being diffuse. In the new generation SX nickel based superalloys, increasing the refractor element ratio leads to increase the heat treatment time and

increase the heat treatment process temperatures. For example, in the first generation SX Ni-based superalloys, a typical solution heat treatment takes about 1 hour at 1300 ºC, while it takes about 30-35 hours at 1366 ºC in the 3rd Generation CMSX-10 superalloy [27].

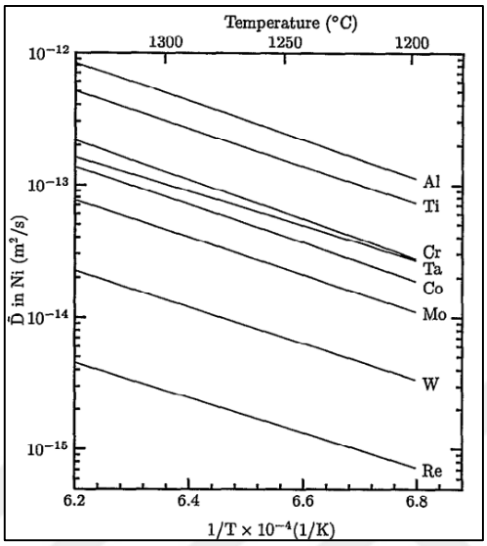

Figure 2.12: Diffusion rate of alloying elements in nickel matrix vs. temperature.

At the end of the solution heat treatment, the samples are usually cooled rapidly using argon gas to prevent coarsening of the precipitates. In solution heat treatment process, a long period of holding at high temperatures results in a pure γ solid solution phase (Figure 2.13a) in FCC structure and also as a result of rapid cooling, the γ' phase (Ni_3 (Al, Ti)) in FCC structure (Figure 2.13b) [33].

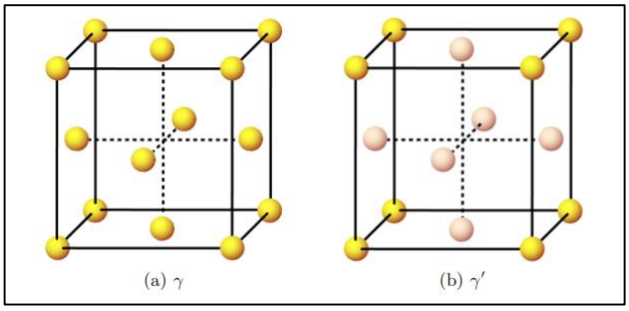

Figure 2.13: Structure of the phases in superalloy, a) γ and b) γ' phases in FCC structure.

When the microstructure is examined after the solution heat treatment process is completed, irregular γ' precipitates can be easily seen in γ matrix. The size of the γ' precipitates directly affects the mechanical properties of the alloy. The size of the precipitate can be controlled by adjusting the cooling rate in solution heat treatment process. During cooling, the precipitates grow and shape to form a cube. In SX superalloys, the size of the precipitates (0.2-5 μm) and morphology are changed with the change of cooling rate (0.02 -100 ºC/s). Figure 2.14 depicts the time-temperature graphs obtained by cooling the CMSX-2 SX superalloy at different cooling rates in solution heat treatment process [29].

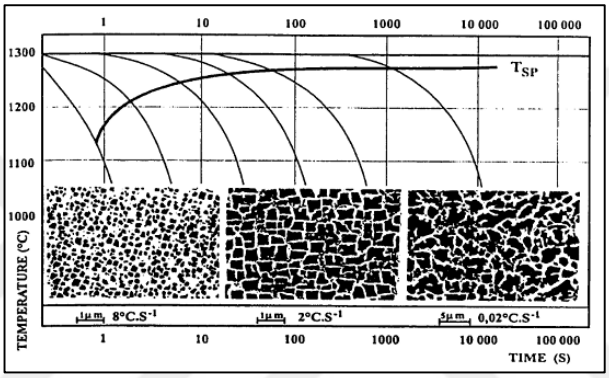

Figure 2.14: Time-temperature graphs obtained by cooling CMSX-2 SX superalloy at different cooling rates in solution heat treatment process.

In order to reduce the cost of the desorption heat treatment, the maximum heat treatment temperature (to ensure faster segregation of the segregating elements) and the minimum heat treatment time should be selected. Because complete dissolution of the eutectic phases and successful microstructure homogenization depends on temperature and duration [27].

2.3.2. Ageing Heat Treatment Process

The ageing heat treatment process performed after the solution heat treatment process is carried out at temperatures below the solvus temperature. The homogeneous nucleation, growth and coarseness of the γ' precipitates form regular and cubic γ' precipitates on γ matrix [27, 33].

The temperature of ageing heat treatment affects the distribution of precipitates, while time affects the size of precipitates. For this reason, the choice of temperature

and time is very important in order to obtain proper morphology, sequence and precipitate size after heat treatment [33].

The ageing heat treatment is carried out at lower temperatures than solution heat treatment, but for a longer period of time. For example, the solution heat treatment of CMSX-4 SX superalloy takes 4 hours at 1080 ºC, while the ageing heat treatment takes 16 hours at 870 ºC. In Figure 2.15, scanning electron microscopy images of the CMSX-4 SX superalloy after solution heat treatment and ageing heat treatment are given [27].

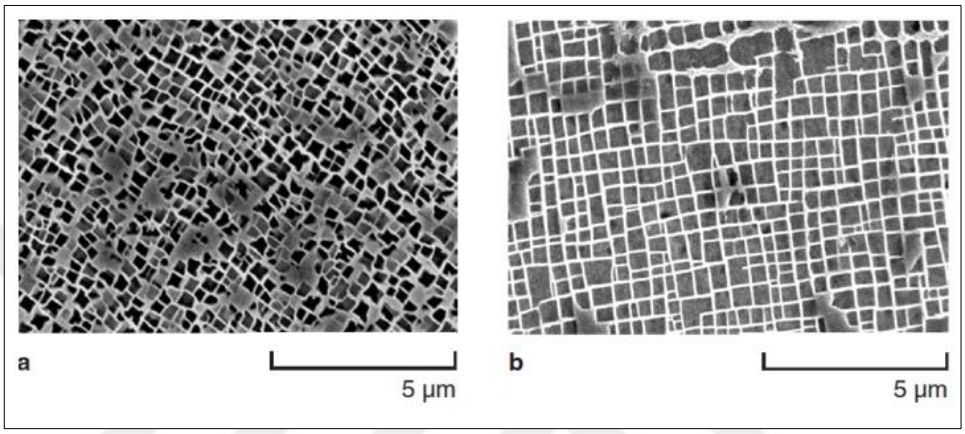

Figure 2.15: SEM microstructures after a) solution heat treatment b) ageing heat treatment of SX CMSX-4 superalloy.

Ageing heat treatment results in cooling in air or in furnace. In order to obtain a homogenized matrix, slow cooling is carried out; while high-volume γ' precipitates in γ matrix cooling in air is carried out. The microstructure obtained by the regular and cubic growth of γ' precipitates increases the creep resistance [33].

3. EXPERIMENTAL STUDIES

In this thesis, CMSX-4 Ni-based single crystal superalloy produced by Cannon-Muskegon is used. CMSX-4 is a 2nd generation Ni-based superalloy which is upgraded from 1st generation Ni-based superalloys CMSX-2 and CMSX-3 via balancing Ta/W ratio, adding about 3% Re, increasing Co content, reducing Cr ratio in order to enhance properties [19]. CMSX-4 is selected because the mechanical properties of this superalloy are suitable for turbine blades and also the production procedures of this superalloy are not complex.

Experimental studies were started with production of the moulds by the investment casting and conventional casting processes, respectively. Two moulds were produced for this thesis to prepare specimens which were required for the tests. Each mould incorporated 12 test rods and totally 24 test rods were produced for the thesis.

3.1. Investment Casting Studies

The moulds for the casting process were designed by using Siemens NX software in desired dimensions after the casting simulations were made by Procast software. The designed model was then made into a wax-bunch model which consists of runners made of wax by Modtech C20 wax injection press and the rods made of ceramic powder by using Voxeljet VX500 3D printer. 3D printer was used in order to eliminate the mould producing process for the model and wax injection press was used because of the cost of PMMA powder which is used in 3D printer. The prepared model is shown in Figure 3.1.

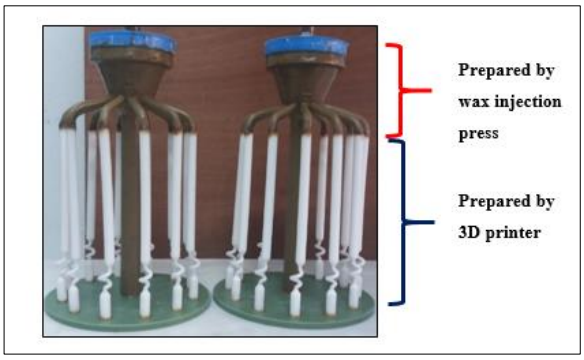

Figure 3.1: Wax - bunch model prepared by 3D printer (the rods) and wax injection press (the runners).

After this step, the wax-bunch model was immersed into the slurry made of fused silica and alumina powder and then the wax was removed by LBBC-1525 autoclave. This process was completed under 10 bar pressure at 200°C in 15 min. At the end, the bunch mould was put into Thermcore box type furnace with 60 kV at 1100°C for 2-2,5 hours to be baked prior to the casting process. At the same time, the wax residual came after autoclave was burnt at this process. The final moulds are seen in Figure 3.2. The gating system of the moulds can be seen from Figure 3.3. All investment casting processes were carried out at TUBITAK MRC.

Figure 3.2: The moulds after baking process.

Figure 3.3: The gating system of the moulds.

For the casting process, “ALD Vacuum Induction Melting (VIM) Furnace”, which was established at TUBİTAK MRC, was used. First, the moulds were put into the furnace and warmed to be ready for the casting. After this process, the casting

process was carried out. The parameters used for the casting process is shown in Table 3.1.

Table 3.1: The parameters used for the casting process.

Vacuum Rate	3.1 x 10^{-3} mBar
Casting Temperature	1530 °C
Mould Temperature	1480 °C
Withdraw Rate	4 mm/min
The amount of the alloy	6,7 kg
The mould size	24cm x 36cm

Figure 3.4 shows a mould after one of two casting treatments. At the end of the process, the ceramic mould was broken down to remove the bunch of specimens from the moulds. Figure 3.5 shows the bunch of specimens after breaking ceramic mould process.

Figure 3.4: A mould after casting process.

Figure 3.5: Bunches of specimens after casting process.

After the casting process was accomplished, the rods were prepared by cutting the bunch into rods. Then, all the rods were cleaned by sand blasting process to remove all residuals emerged from ceramic mould.

After preparation of the rods, non-destructive inspection test was applied on each rod in order to find out if any volumetric defect occurred within prior to the mechanical tests. YXLON MU2000-D CT Radioscopy & CT (Computed Tomography) test system with W anode/cathode X-Ray tubes was used for the test. The important parameters regarding the test system are shown in Table 3.2. An inspection test result is shown in Figure 3.6.

Table 3.2: The parameters used at radioscopy & CT test system.

Device	YXLON MU2000-D CT
Voltage	280 kV
Current	2,5 mA
Focal Spot Size	0,4 mm
Filter	2,5 mm brass filter
Focus detector distance (FDD)	900 mm
Focus object distance (FOD)	450 mm

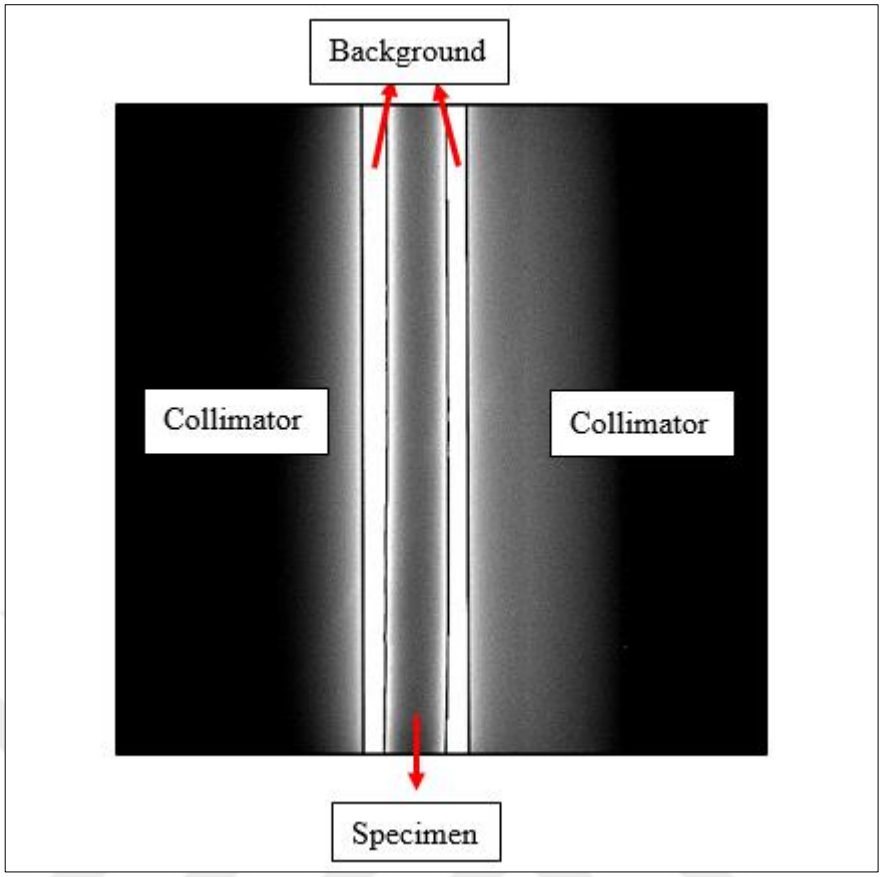

Figure 3.6: Non-destructive test applied on a specimen.

As can be seen from Figure 3.6, there is no volumetric defects observed on specimens after casting process.

3.2. Heat Treatment Studies

Two heat treatment processes selected for the thesis are shown in Table 3.3. The first process is the standard heat treatment process of CMSX-4 superalloys. The heat treatment process of PWA 1480 was selected as the modified heat treatment process in order to leave eutectic phases unsolved in solution and investigate the effects of eutectic phases with their mechanical effects on CMSX-4 superalloy. This process is taken from the study made by Wilson et. al. [34]. All heat treatment processes were performed in Nabertherm box type furnace under argon atmosphere.

Table 3.3: Heat treatment processes and steps applied in this thesis.

	Heat Treatment Steps
Standard Heat Treatment Process of CMSX-4 (A)	Solution Heat Treatment: 1277°C (2h) + 1288°C (2h) + 1296°C (3h) + 1304°C(3h) + 1313°C (2h) + 1316°C (2h) + 1318°C (2h) + 1321°C (2h)+AC [Heating Ramp 1°C/min] Ageing 1: 1140°C (2s) + AC Ageing 2: 871°C (20s) + AC
Modified Heat Treatment Process (B)	Solution Heat Treatment: 1210°C (2h) + 4,5 h ramping + 1285°C (2h) + 1h 12 min ramping rate + 1287°C (30 min)+AC Ageing 1: 1140°C (6s) + AC Ageing 2: 871°C (20s) + AC

The specimens are numbered as shown in Table 3.4. Specimen codes named with A (Standard heat treated specimens) and B (Modified heat treated specimens) to indicate the heat treatment process applied on specimens. The number after A and B, indicates the test number. For example, "HT-982-B2" is refers to "2nd modified heat treated specimen used for high temperature tensile test applied at 982 °C".

Table 3.4: Specimens used in this thesis.

Specimens	**Specimen Code**	**Applied Heat Treatment**
RT Tensile Test Specimens	RT-A1	Std. CMSX-4
	RT-A2	
	RT-B1	Modified
	RT-B2	
HT Tensile Test Specimens (for 982 °C)	HT-982-A1	Std. CMSX-4
	HT-982-A2	
	HT-982-B1	Modified
	HT-982-B2	
HT Tensile Test Specimens (for 1038 °C)	HT-1038-A1	Std. CMSX-4
	HT-1038-A2	
	HT-1038-B1	Modified
	HT-1038-B2	
Stress Rupture Test Specimens	SR-A	Std. CMSX-4
	SR-B	Modified
Microstructure Specimens	M-A	Std. CMSX-4
	M-B	Modified

Microstructure specimens are numbered in themselves. Table 3.5 shows the classification of microstructure specimens in regarding with the cross sections taken from the rods.

Table 3.5: Microstructure specimens used in this thesis.

Transverse Section		Longitudinal Section	
Specimen	Heat Treatment	Specimen	Heat Treatment
M-A-T	Std. CMSX-4	M-A-L	Std. CMSX-4
M-B-T	Modified	M-B-L	Modified

3.3. Metallography Studies

The specimens were prepared via cutting the rods to specimens for microstructural analysis by using ATM Brillant 220 cutting machine. After that, the specimens were mounted with ATM Opal 460 model hot mounting press and then, they were grinded and polished by Struers Roto-Pol 25. The specimens were grinded for 90 seconds using 120, 240, 320, 400, 600, 800, 1200, 2500 SiC grinding papers, respectively. After rough polishing bilaterally with ATM Diamantschmiermittel diamond lubricant for 45 seconds, the specimens were fine polished with Buehler Masterpolish 0,05 μ Colloidal Silica & Alumina polisher.

For etching process, fresh Glyceregia (50 ml glycerol + 30 ml HCl + 20 ml HNO_3) was prepared and the specimens were electrically etched for 5 sec under 4A using Struers Lectropol-5. Glyceregia was used to observe the general microstructure of CMSX-4 superalloy and also has a good view effect on SEM.

After etching process, optical micrographs were taken by Nikon Eclipse L150 microscopy. For image analysis, such as SDAS calculation and phase analysis, Java-based software ImageJ was used. Microstructures were also observed by using Jeol JSM-6510LV SEM at TÜBİTAK MRC and Philips XL 30 SFEG SEM at Gebze Technical University. Specimens for SEM were used after platinizing (30-40 μm) process.

3.4. X-Ray Diffraction Studies

Laue X-ray diffraction method was used in order to check the single crystallinity of the specimens at room temperature. The test carried out by Proto XRD Laue COS device with 40 kV accelerating voltage and 30 mA the tube current. Exposure time was 6500ms with 8 frames.

The specimens also were analysed by using Rigaku SmartLab Multipurpose X-ray diffraction (XRD) system.

3.5. Simulation Studies

Java-based material properties software, JMAT Pro v8.0 was used to calculate phase equilibrium diagrams of CMSX-4 via using the SX database. Phase transformations diagram for CMSX-4 was drawn by thermodynamic calculations made by JMAT Pro. At the same time, elemental composition changes by temperature for γ and γ' are calculated.

3.6. Mechanical Test Studies

For this thesis, room temperature (RT) and high temperature (HT) tensile tests, stress rupture tests were carried out to observe the effects of heat treatment processes on mechanical properties of CMSX-4.

3.6.1. Tensile Test

Tensile tests were performed both at room temperature and high temperature. Zwick/Roell Z600 (600kN) Universal machine was used to carry out the test using ISO 6892-1 (2016) standard method A under 100N pre-load with the velocity of 0,0067 s^{-1}. Epsilon 3448 high temperature extensometer was used during the test. 982°C and 1038°C temperatures were selected to apply the tensile test on specimens. These temperatures selected from the study made by Fullagar et.al. [8] in order to compare the results obtained this thesis. On the other hand, these temperatures are in the temperature range where CMSX-4 alloys show desired properties.

The dimensions of the specimens were measured before and after each accomplished test. The yield strength at 0.2 % plastic strain deformation $R_{p0.2}$, tensile strength Rm and elongation %ε were determined by the software.

3.6.2. Stress Rupture Test

Stress rupture tests were performed in ATS WIN CCS creep test machine. The specimens were prepared with regards to ASTM E139-11 standard.

The stress rupture tests were performed at 982°C under 345 MPa load with -3°C /+3°C sensibility. After the results obtained from tensile tests, it was decided to perform these tests at 982°C.

3.6.3. Hardness Test

Hardness test studies were carried out using Qness Micro Hardness tester under 1 kg load. The results were obtained from transverse sections of two heat treated specimens and as-cast specimen.

4. RESULTS & DISCUSSION

4.1. Confirmation of Single Crystal (SX) Formation

Single crystal formation was observed by Laue XRD method. It is predicted that the single crystal zone axis is equal to the [001]. According to Laue X-ray diffraction pattern, which is shown in Figure 4.1, all the reflection spots (in grey colour) are clear and sharp. The green circles of the numerical simulation, which are shown in Figure 4.1b, match the experimental diffraction pattern with rotation angle of gamma which is equal to 1.60°. As a result, it is oriented in [001] direction with single crystal formation.

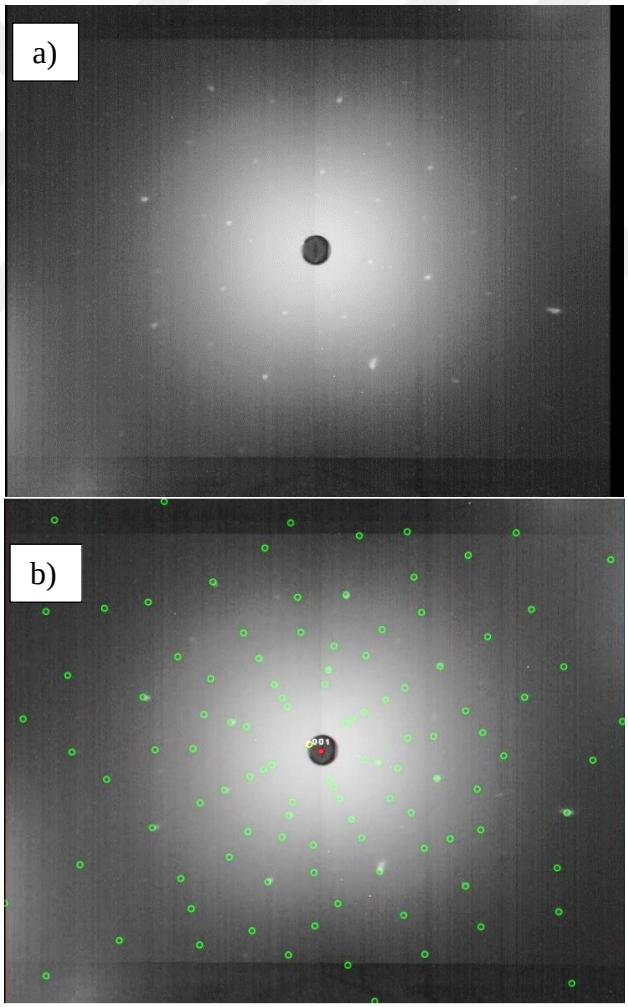

Figure 4.1: The laue diffraction diagram from single crystal zone axis [001] of CMSX-4, a) laue diagram b) laue diagram with diffraction pattern.

The specimens also were analysed by using Rigaku SmartLab Multipurpose X-ray diffraction (XRD) system via using Time Delay Integration (TDI) scan by 2D mode which is shown in Figure 4.2.

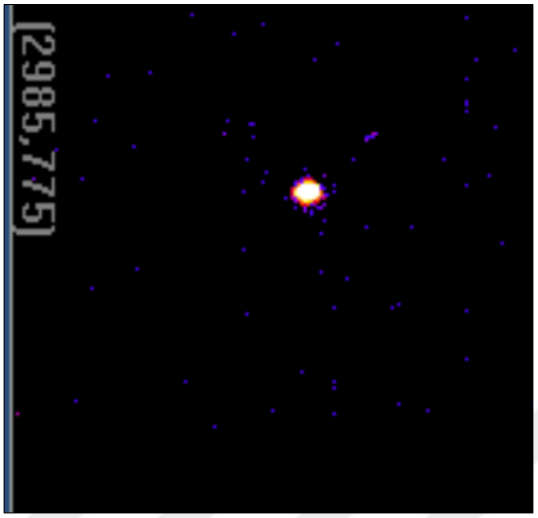

Figure 4.2: Single shot image by TDI (Time Delay and Integration) scan by 2D mode of HyPix-3000.

Two analysis were carried out on the crystallographic planes (001) of the specimen and the XRD profile with results are shown in Figure 4.3 and Table 4.1, respectively.

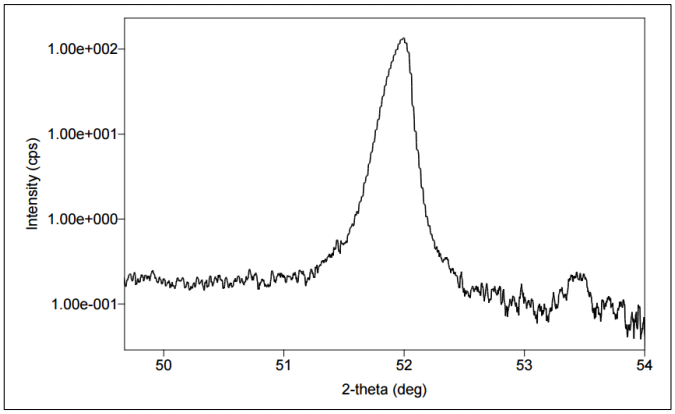

Figure 4.3: XRD analysis on crystallographic planes (001).

Table 4.1: XRD analysis results.

Analysis No	2-θ (deg)
1	52.0064
2	53.47

The X-ray investigations (Figure 4.2) of CMSX-4 showed only one reflection at 52° and 53° on the 2-θ scale (Table 4.1). These results indicate that the material has a single crystalline microstructure with no grain boundaries.

4.2. Thermodynamic Studies

Thermodynamic calculations of CMSX-4 simulated by JMAT Pro and the phase transformation changes vs increasing temperature are shown in Figure 4.4.

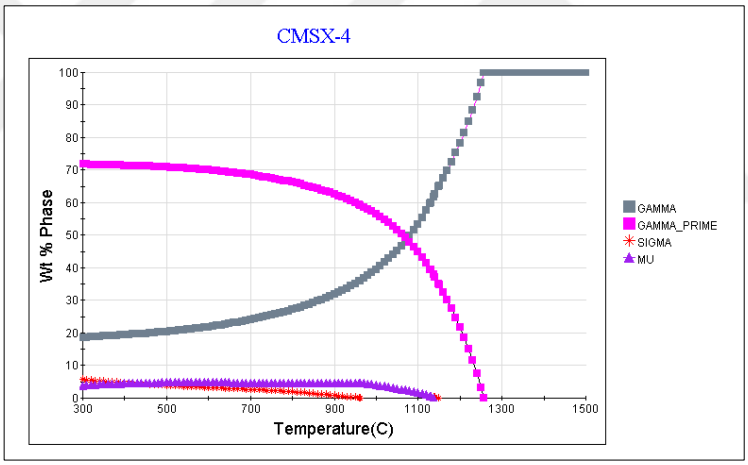

Figure 4.4: Phase equilibrium-Temperature diagram simulated by JMAT Pro.

According to the calculations made by JMAT Pro, γ matrix and γ' precipitates and small amount of μ and σ phases are present in the graph. After 900°C, the amount of γ' precipitates slightly reduces and close to 1200 °C these precipitates dissolve in γ-matrix completely.

Figure 4.5 and Figure 4.6 illustrate elemental change by increasing temperature in γ' precipitates and γ-matrix respectively.

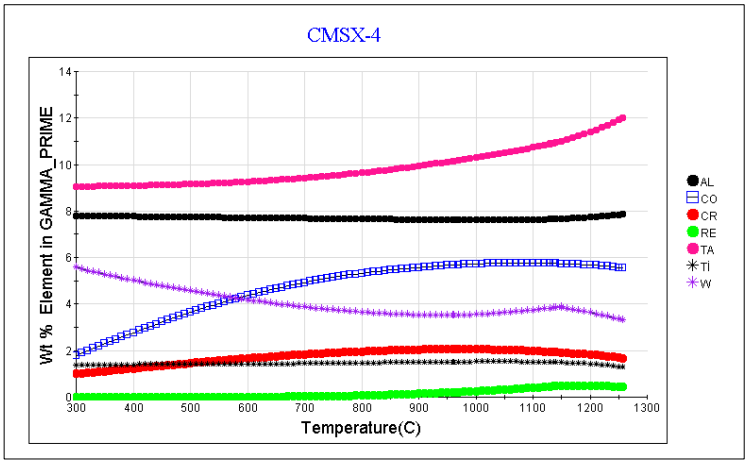

Figure 4.5: Elemental distribution in γ'-precipitates by increasing temperature simulated by JMAT Pro.

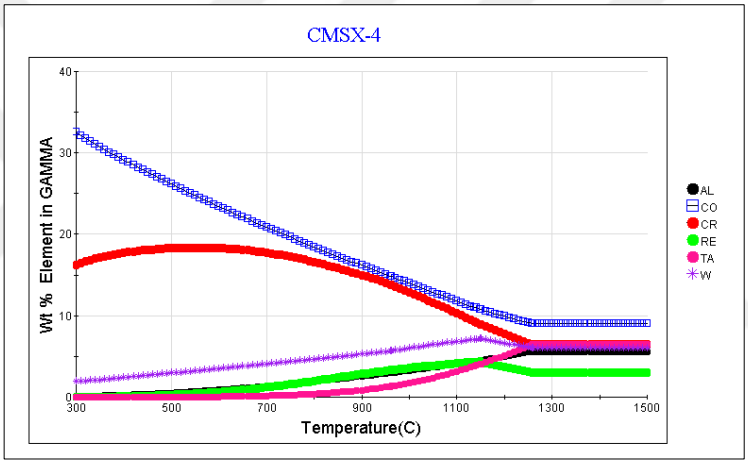

Figure 4.6: Elemental distribution in γ-matrix by increasing temperature simulated by JMAT Pro.

As can be seen from Figure 4.5, γ' precipitates contain Al, Ti, Ta elements higher than 6% wt. at higher temperatures. Figure 4.6, illustrates the elemental distribution in γ- matrix by increasing temperature.

According to the calculations, γ' precipitates that effect not only the hardness of the materials but also mechanical properties are changing with the size of the precipitates. Figure 4.7 illustrates simulation graph of the effects of the size of the γ'-precipitates on the hardness and mechanical properties of CMSX-4 at 982°C which is in the range of operating temperature of a turbine blade.

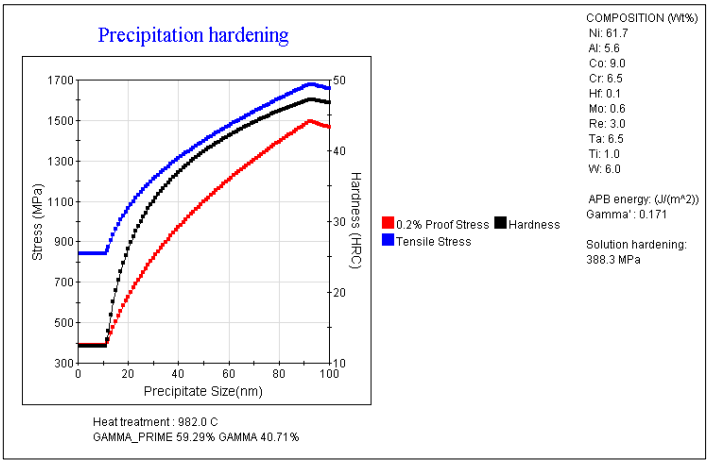

Figure 4.7: Simulation of the size effect of precipitates in terms of the hardness and mechanical properties of CMSX-4.

4.3. Microstructural Characterization

4.3.1. Optical Microscopy (OM)

According to the first investigations, undesired casting defects were observed. The Si-based defects are clearly seen in the micrographs shown in Figure 4.8.

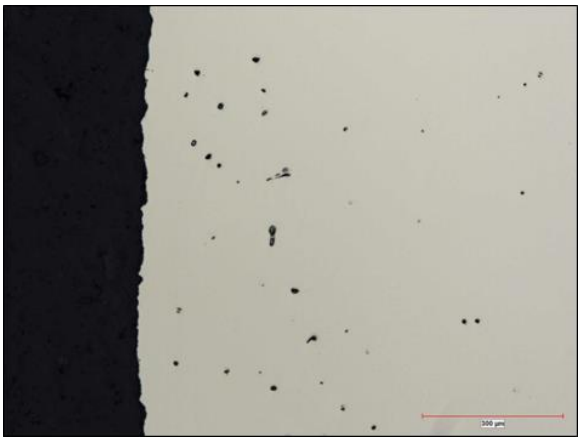

Figure 4.8: Si-based defects.

It is considered that the reason of these Si-based residuals come from the billets. The waterjet cutting system (CT waterjet with 3800 bar pressure) was used to cut the billets to required size for the casting process and Si-based abrasive sand was used while cutting. It is predicted that this process could be the reason of these defects. These defects were observed mostly at the edge of the specimens. EDS (Energy

Dispersive X-ray Spectroscopy) analysis result is shown in Figure 4.9. The analysis was taken from the defect and matrix. The results proved that these defects are based on SiC which came from during cutting.

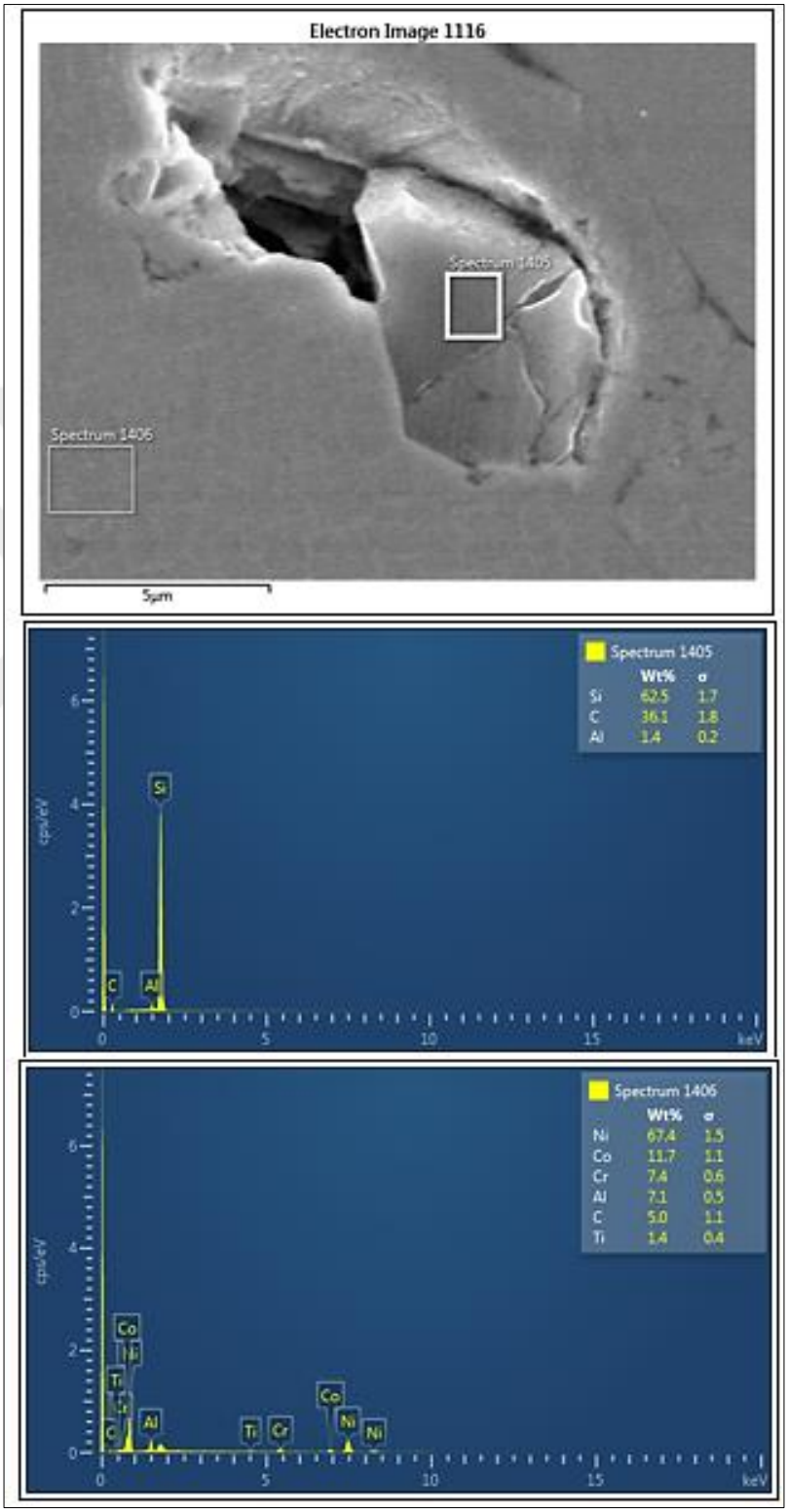

Figure 4.9: EDS analysis result

There are a few recrystallized grains observed at the edge of the specimens. This recrystallization problem is the formation of the grains which is oriented randomly at the edge of the surface, during heat treatment process. It is predicted that, the cold work made during sand blasting process (sand blasting process was used to remove the ceramic residuals after casting) is the reason of the recrystallization problem. Another reason of recrystallization is the differential thermal contraction between the components. The temperature difference between the mould, melt metal and ceramic cores also results in the recrystallized grains occurred at the surface of the component [27, 35]. Figure 4.10 shows the recrystallization defects occurred in this study.

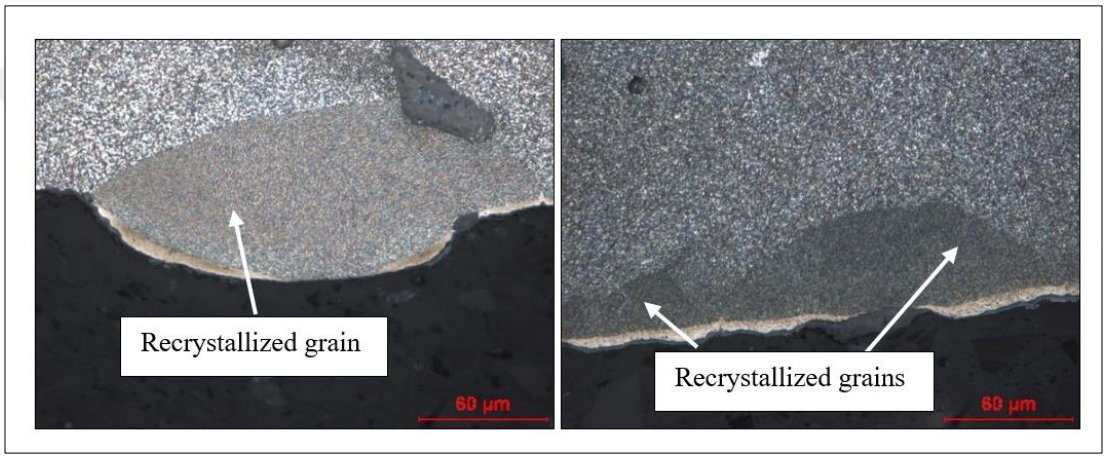

Figure 4.10: Recrystallized grains.

Zhang et. al. [36] studied regarding surface recrystallization of single crystal Ni-based superalloys. They indicate that, the annealing temperature affects the morphology of the recrystallized grains. Cellular recrystallized grains can be observed below γ′ solvus; but above solvus, appropriate formed grains are resulted in recrystallization. Recrystallized grains occur in dendritic core regions and grow inwards along dendritic cores. Recrystallized grain boundaries move through interdendritic areas after dissolution of coarse γ′ precipitates and γ/γ′ eutectic regions in interdendritic regions. They also claimed that the dissolution of primary γ′ precipitates effect the recrystallization behaviour of SX superalloys. The studies made by Wang et. al. [37] and Wang et. al. [38] indicate that the nucleation and grain growth behaviour of recrystallized grains are related to the dislocation density with eutectic regions. The high dislocation density in eutectic/γ' and at eutectic/matrix interfaces promotes the nucleation of recrystallized grains. If the dislocation density within

eutectic regions is high enough, the eutectics tend to be recrystallized when a recrystallized grain boundary moves by. If it is low, the recrystallized grain boundary is pinned at the eutectic.

On the other hand, there are a few twin formations observed in recrystallized grains. According to the study made by Xiong et. al., [39] this twin problem occurred in equiaxed recrystallized grains comparison to the cellular recrystallized grains because of the lower stacking fault energy of γ matrix. Twin formations observed in this thesis are shown in Figure 4.11.

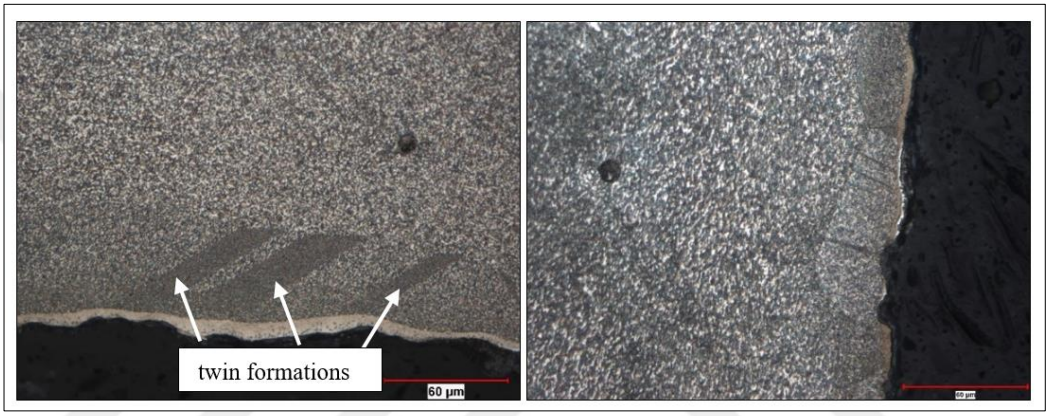

Figure 4.11: Twin formations in recrystallized grains.

Another observed defect is the interaction between the molten metal and the ceramic mould. Figure 4.12 shows this interaction problem. Ceramic residuals passed into metal during casting process, and this results in contaminations in final material.

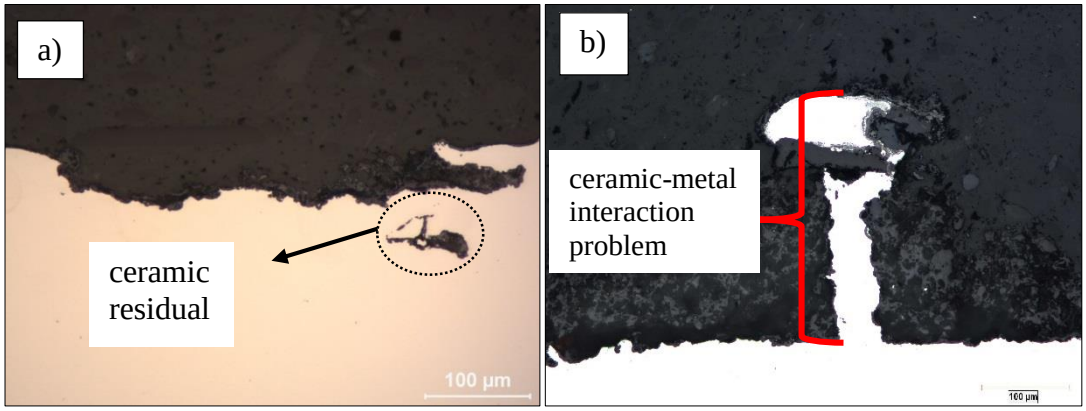

Figure 4.12: Ceramic-metal interactions at the surface of specimens a) ceramic residual problem b) ceramic-metal interaction problem

General microstructure investigations were taken from as-cast and heat treated specimens (M-A and M-B, respectively) after etching with gligeregia. The micrographs at the magnification of 5X for as-cast, 2,5X for heat treated specimens from their transverse and longitudinal sections are shown in Figure 4.13.

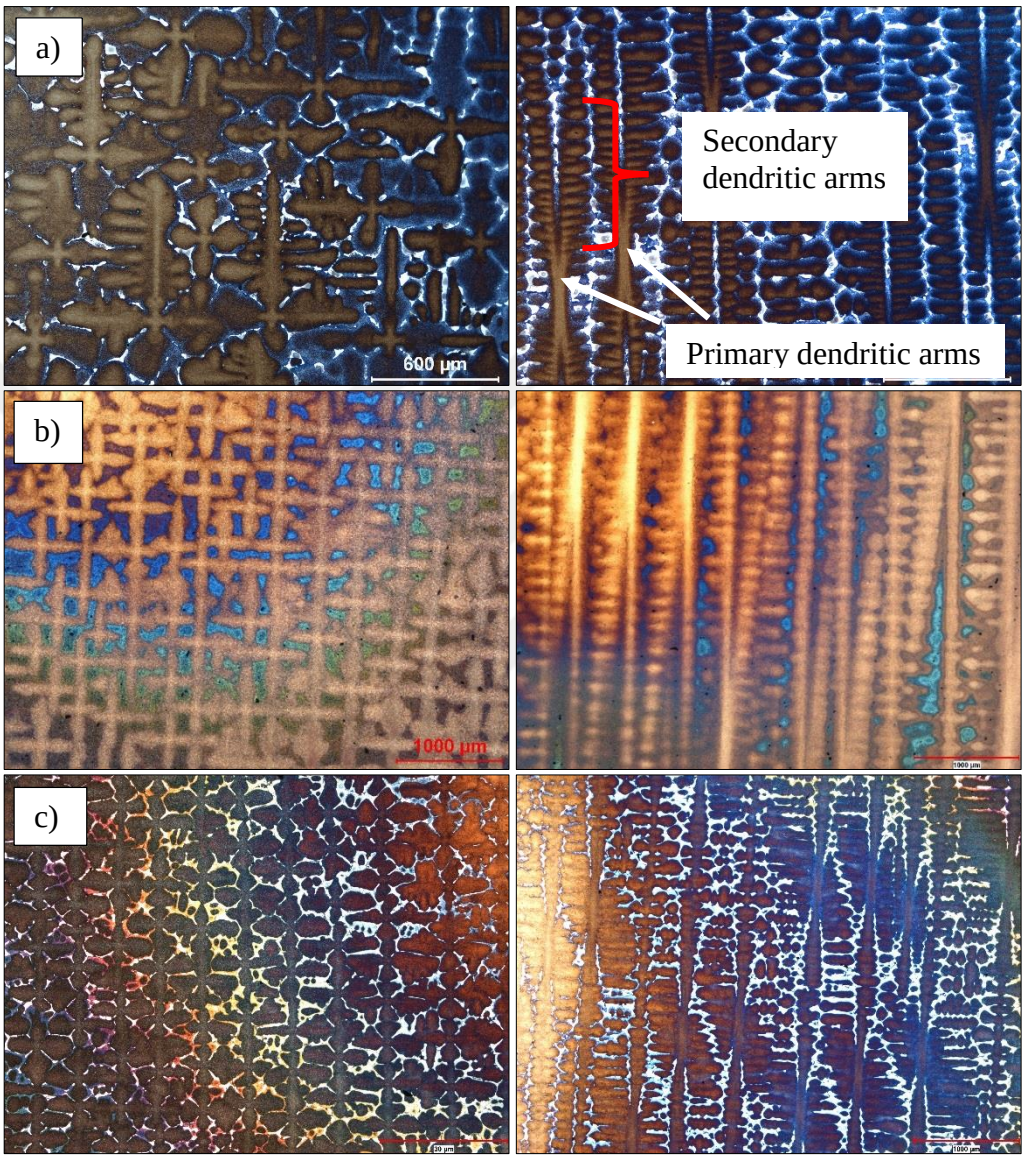

Figure 4.13: The micrographs of a) as-cast specimen at the magnification of 5X b) M-A c) M-B specimens at the magnification of 2,5X from their transverse (left) and longitudinal (right) sections.

The microstructures of as-cast specimen in 5X magnification show the dendrites and the eutectic regions between these dendrites clearly. The primary dendritic arms with secondary dendritic arms are indicated in the figure. Modified heat treatment shows the same effect in the microstructure. Eutectic regions are mostly located

between secondary dendritic arms and at the edges of these dendrites. The effect of standard heat treatment process is not the same as modified heat treatment process. As can be seen from the related figures, after long time exposure to high temperatures, eutectic regions dissolved into matrix and therefore the eutectic regions cannot be seen throughout material. Similar microstructural properties are obtained from the study achieved by Wilson et. al. [34]. They aimed to see the effect of solution heat treatment process on microstructural changes. In their study, they observed γ/γ' eutectic regions and dendrite cores with secondary arms easily after modified heat treatment process.

Rzyankina et al. [26] also studied the standard heat treatment of CMSX-4. They were aimed to see the effect of heat treatment in terms of microstructural, hardness and crystallography orientation of CMSX-4. After solution heat treatment, ageing-1 and ageing -2 processes they observed the microstructural changes in CMSX-4. After solution heat treatment process, they observed that the dendritic cores with their dendritic arms can be identified easily. They also observed that ageing-1 effects γ/γ' coherency throughout of material but not enough yet to stabilize; and after ageing-2 process, γ/γ' eutectic regions were dissolved completely.

According to the study made by Karunaratne et. al. [40], during solution heat treatment process, homogenising of dendritic and interdendritic regions occur at different rates. They also noted that, in CMSX-4 superalloys, Co, Cr, Re, W segregate to the dendritic cores with Al, Ni, Ta, Ti partitioning to the interdendritic regions. In addition to this, backdiffusion effects can occur during solidification process. Kruk et al. [41] studied where these elements are segregated in. The results show that Co, Cr and Re have a relatively high solubility in γ matrix, while Ni and W present in both γ and γ′ precipitates. Al, Ti and Ta elements are partitioned to the γ′ phase. An advanced study regarding elemental segregation made by Hemmersmeier et. al. [42]. According to this study, after standard heat treatment process Re and W elements were detected in the matrix of the dendrites compared to the interdendritic regions. γ′ precipitates and their morphology are more stable in dendrites and therefore the strength of the dendrites is higher.

The precipitation process of γ′ precipitates are important parameters that have influence on mechanical properties of superalloys. According to the study made by Ges et al. [43] the heating rate strongly influences the initial and final temperature of precipitation process, then effecting mechanical properties.

Figure 4.14 shows the microstructures at the magnification of 10X for each condition.

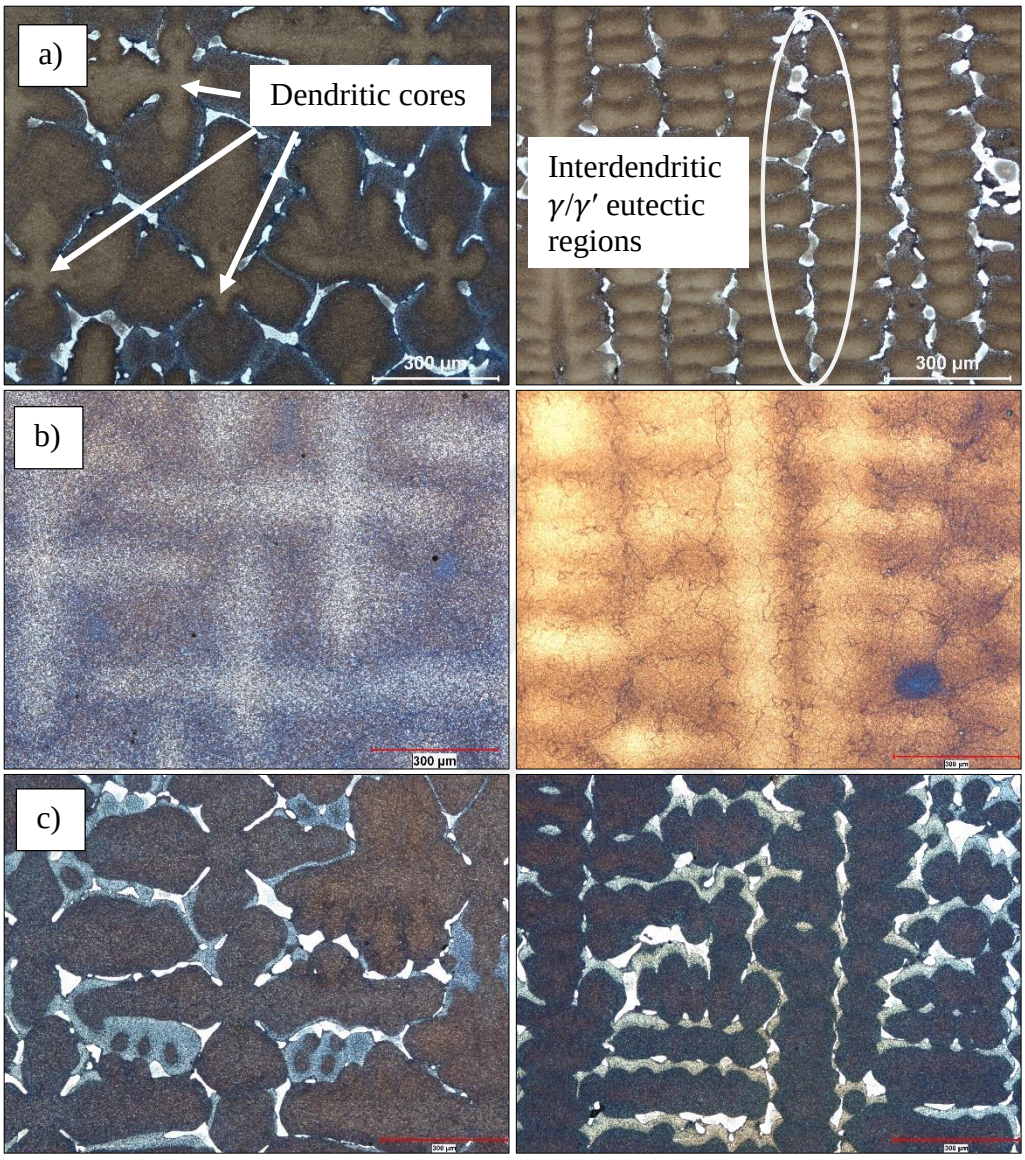

Figure 4.14: The micrographs of a) as-cast b) M-A c) M-B specimens at the magnification of 10X from their transverse (left) and longitudinal (right) sections.

As-cast microstructures show dendritic cores with the γ/γ' eutectic precipitates or eutectic islands which occur in the interdendritic regions (Figure 4.14a). As can be seen from Figure 4.14b, standard heat treatment process dissolved these eutectic phases and the dendrite cores are not seen clearly. Longitudinal section of M-A specimen shows elemental segregation like capillaries after dissolution of eutectic regions. These eutectic regions started to dissolve into matrix shown as in grey colour

in Figure 4.13c. The undissolved eutectic regions (in white colour) left between secondary arms.

Figure 4.15 shows the capillary lines in micrographs at the magnification of 20X. As can be seen that, the capillary like lines here are more sensible. They cannot be identified in transverse section specimen because in transverse section, they seem like points and not big enough to be observed by optical microscopy.

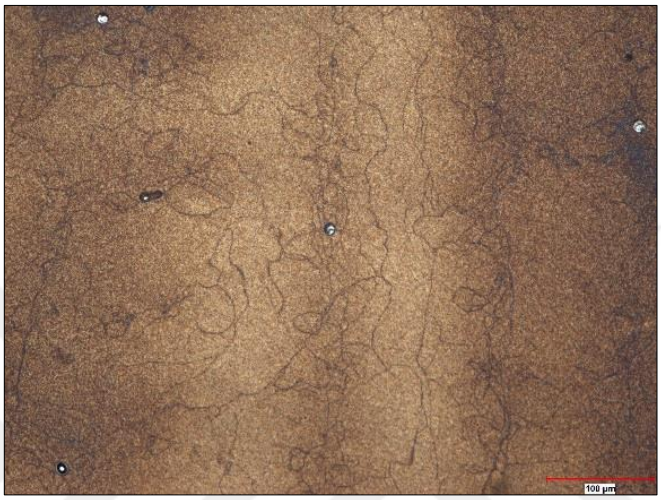

Figure 4.15: The micrograph of M-A at the magnification of 20X from its longitudinal section.

Figure 4.16 shows the micrographs of as-cast and M-B specimens at the magnification of 50X from their transverse and longitudinal sections. As can be seen from Figure 4.15, the eutectic regions after modified heat treatment process started to dissolve and easily be observed at the magnification of 50X. The morphology of eutectic regions is not same before and after heat treatment process. The modified heat treatment process is not enough yet to dissolve all these eutectic regions. The eutectic regions first start to dissolve as coarse γ' precipitates and then transform to fine γ' precipitates which are going to dissolve in γ matrix later.

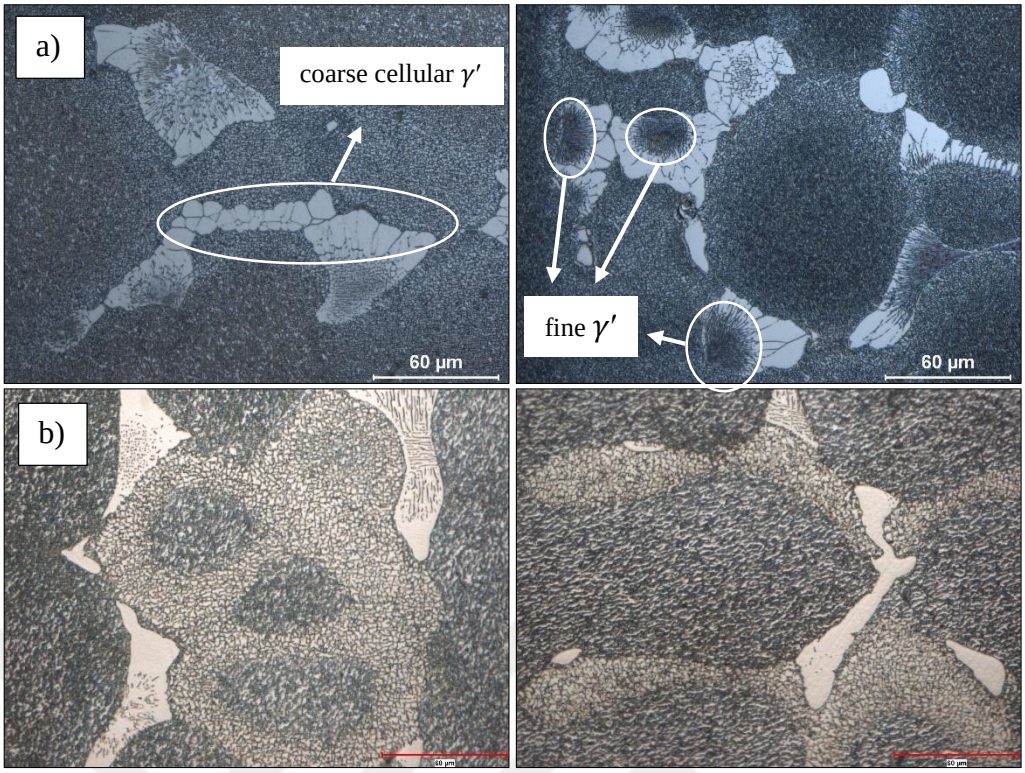

Figure 4.16: The micrographs of a) as-cast b) M-B specimens at the magnification of 50X from their transverse (left) and longitudinal (right) sections.

The percentage of eutectic regions after modified heat treatment process was calculated by ImageJ software via thresholding eutectic regions illustrated in Figure 4.16. The volume percent of eutectic regions is calculated about 10%. Eighty micrographs at the magnification of 10X were used for the calculations.

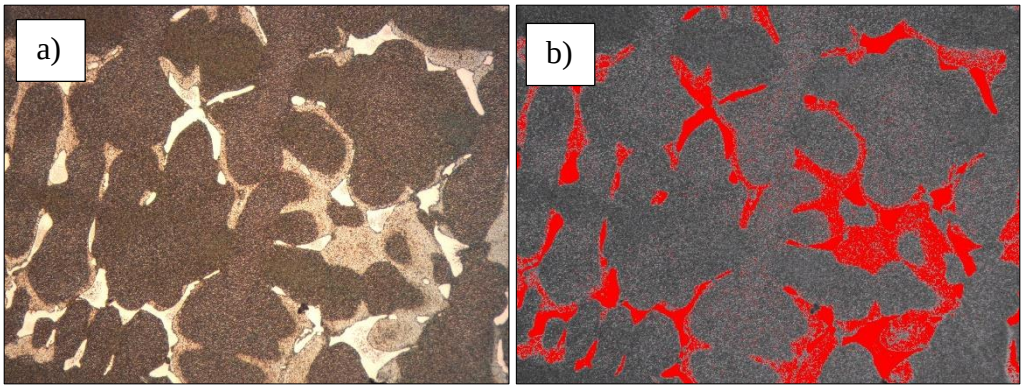

Figure 4.17: Thresholding eutectic regions with ImageJ a) before thresholding b) after thresholding.

4.3.2. Scanning Electron Microscopy (SEM)

The as-cast microstructures of CMSX-4 are shown in Figure 4.18. The γ' precipitates are not ordered regularly within material and they are not in desired shape. The γ/γ' eutectic regions and coarsened γ' precipitates are located throughout specimen.

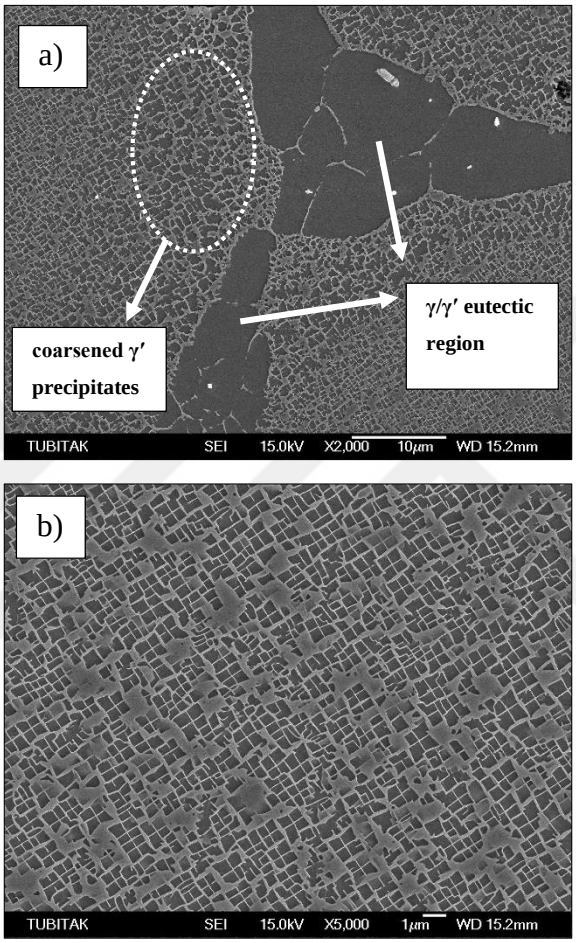

Figure 4.18: General microstructure of as-cast CMSX-4 specimen at the magnifications of a)2000X and b)5000X, respectively.

The general microstructure of CMSX-4 is shown in Figure 4.19 after standard heat treatment process.

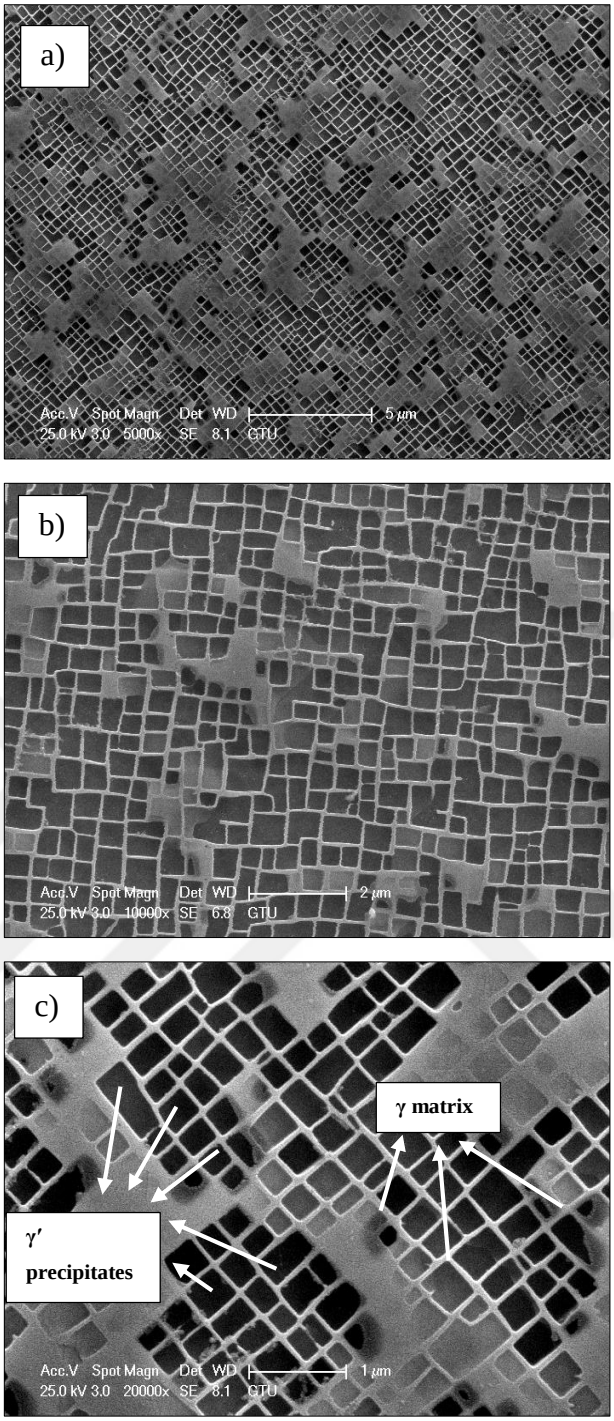

Figure 4.19: General microstructure of CMSX-4 after standard heat treatment process at the magnifications of a) 5000X, b)10000X and c)20000X, respectively.

As can be seen from Figure 4.19 that, γ' precipitates ordered regularly in proper shape and the size of γ' precipitates vary approximately 0.4 - 0.5 μm which has influence on mechanical properties at different temperatures [44]. Because of exposing the specimen to high temperatures for long time, the eutectic regions dissolved

completely and the coarsened γ' precipitates are not seen throughout material. The size of γ' precipitates are close to the results calculated by Evans et. al. [45].

The general microstructure of CMSX-4 after modified heat treatment process is shown in Figure 4.20.

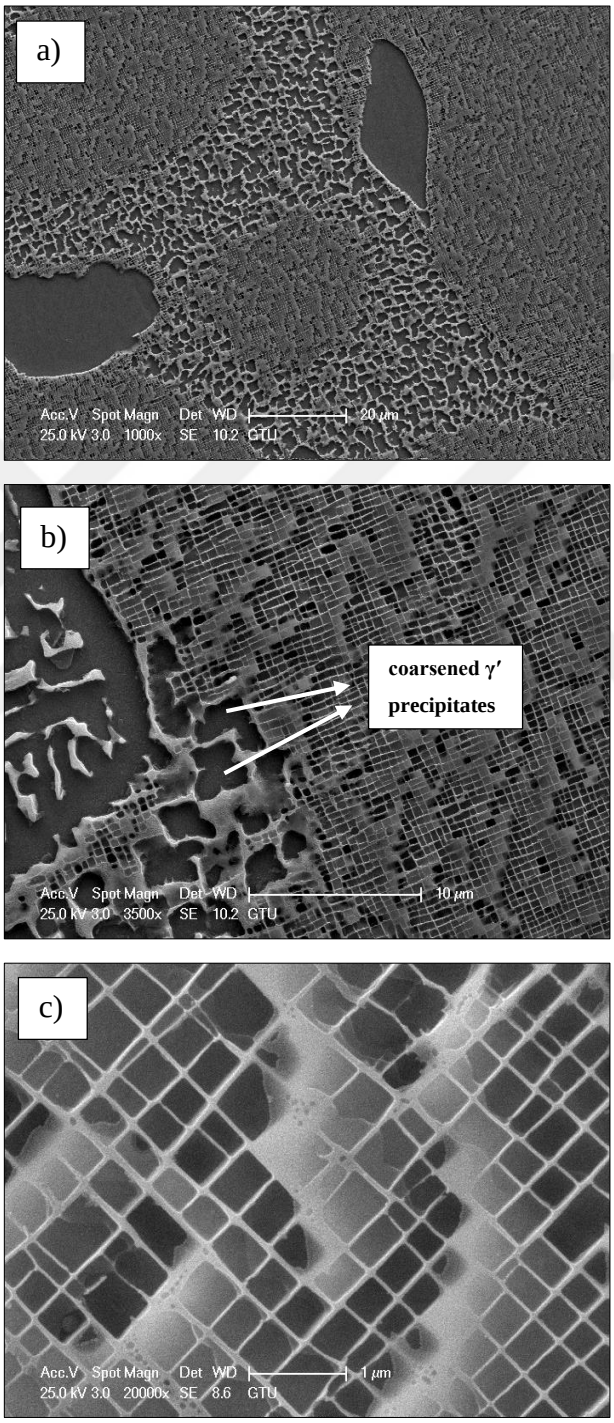

Figure 4.20: General microstructure of CMSX-4 after modified heat treatment process in magnifications of a) 1000X, b) 2000X and c) 20000X, respectively.

The micrograph in 1000X shows some γ/γ' eutectic regions with coarsened γ'-precipitates. The time in modified heat treatment process is not enough to dissolve all eutectic regions into matrix. Distinguishable boundaries were occurred by coarsened γ' precipitates between eutectic regions and dendrites. In the study made by Wilson et al. [34] they observed the same microstructural morphologies.

At the edges of the specimens, the formation of spherical γ' precipitates is observed. The temperature gradient between the surface and the material resulted in this morphology. The high temperature at the surface effects γ' precipitates kinetically and hence their morphology changes from cubic form to spherical form. Figure 4.21 shows this morphological change.

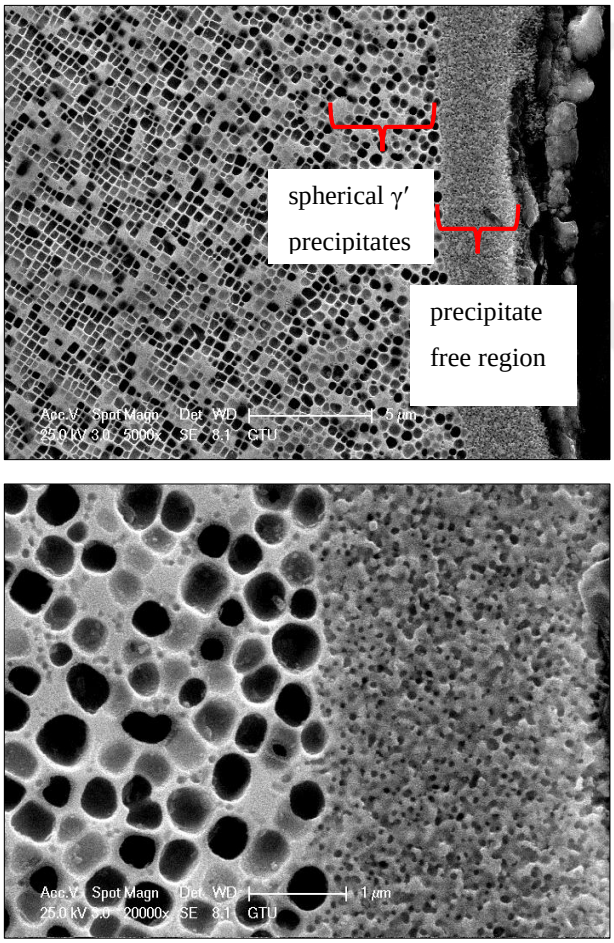

Figure 4.21: Spherical gamma prime precipitates at the edge of the samples at the magnifications of a)5000X and b) 20000X, respectively.

The grain formation after recrystallization is shown in Figure 4.22.

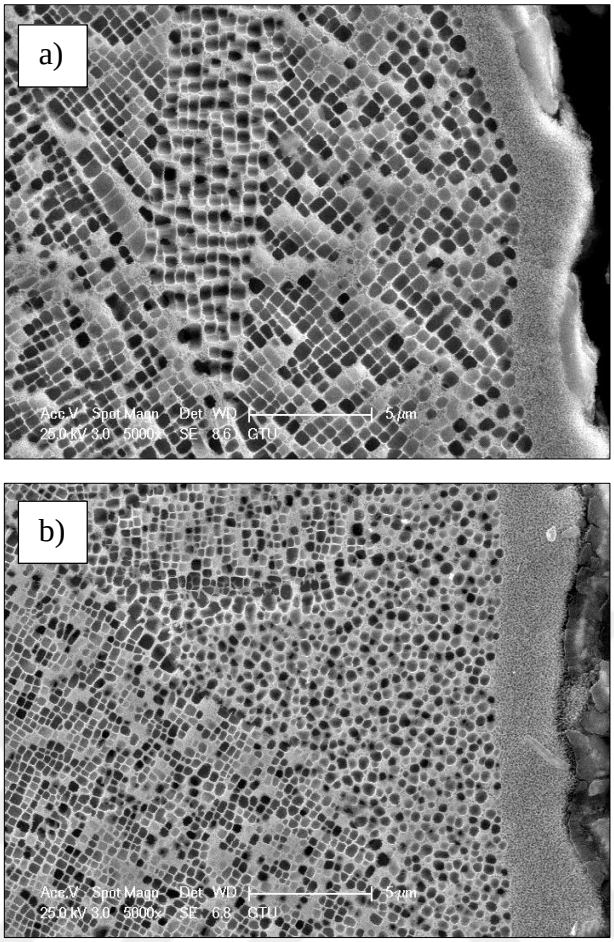

Figure 4.22: Grain formation at the edge of the specimens a) M-B b) M-A

New grain formations with different orientations are occurred at the edge of the specimens because of the internal stresses at the surface of the specimens. Heating specimen to higher temperatures release this energy and this energy results in the formation of new grains.

The volume percent of γ-matrix and γ' precipitates are important parameters for SX superalloys. Across a wide range of temperature and levels of applied stress, creep deformation on the microscale is restricted to the γ channels which lie between the γ' precipitates. Hence, the dislocations do not penetrate the γ' precipitates. This results with a reduced fraction of γ-matrix which yields improved properties. Creep performance does not increase monotonically as γ' fraction increases. Hence, an alloy with 70% γ' performs greater than the other one with 100%. This is because of the strengthening effect of γ/γ' interfaces which prevents creep deformation [1]. The volume fraction of γ and γ' precipitates are calculated from SEM micrographs by ImageJ and the results are shown in Table 4.2.

Table 4.2: Volume fractions of γ and γ' precipitates calculated by ImageJ.

Specimens	M-A		M-B	
	% γ'	% γ	% γ'	% γ
Volume fractions	70,41	29,60	71,73	28,27
Standard Deviation	3,37		2,30	

The desired volume fraction of γ and γ' precipitates were obtained after the calculations. In the study made by Lapin et. al. [46], volume fraction of γ′- precipitates range from 62 to 70 vol %. They also indicated that the volume fraction and the size of γ′ precipitates effect the vickers hardness at the same time mechanical parameters of CMSX-4 superalloys. With decreasing volume fraction and increasing overall size of γ′ precipitates, the vickers hardness and yield strength decrease.

4.4. Mechanical Characterization

4.4.1. Tensile Test

To observe the mechanical effects of the heat treatment processes, tensile tests were performed on heat treated specimens at RT, at 982°C and at 1038°C. As mentioned before, these temperatures are selected because they are in the range of operating temperature of turbine blades.

Two specimens were prepared for each heat treatment process and for each tensile test. Figure 4.23 and Figure 4.24 show the stress-strain behaviour of RT-A and RT-B specimens at room temperature, respectively and the results obtained from these tests are shown in Table 4.3.

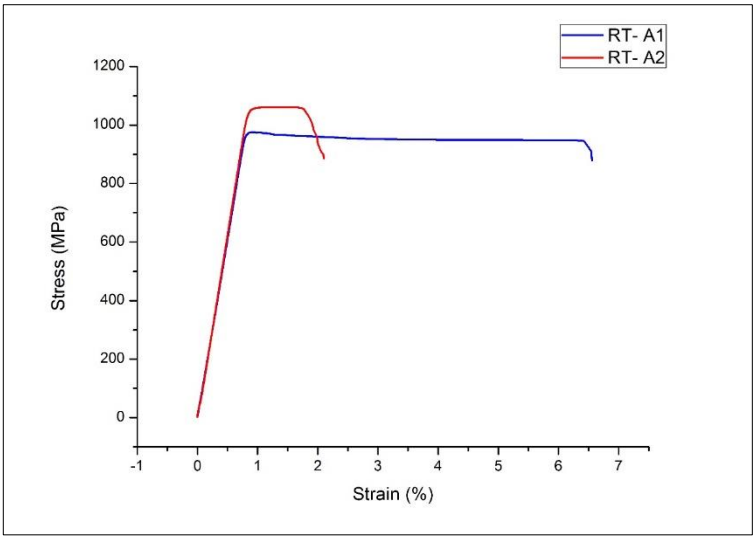

Figure 4.23: Stress-strain behaviour of standard heat treated specimen at room temperature.

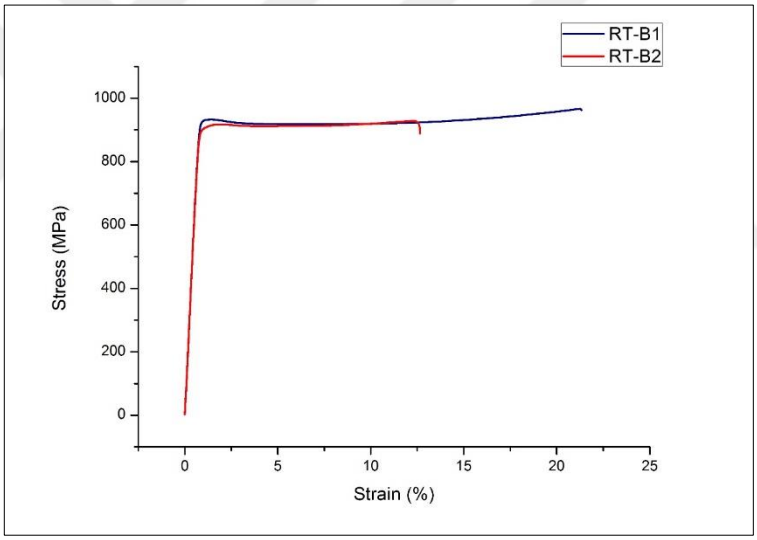

Figure 4.24: Stress-strain behaviour of modified heat treated specimen at room temperature.

Standard heat treated specimens show different characteristic properties at room temperature tensile test. It is determined from Figure 4.23 that the elongation values have a difference between two results. It is considered that this difference is the result of strain hardening mechanism in the region of plastic flow. The yield strength of RT-A1 is lower however have a higher elongation. Epishin et. al. [47] studied microstructural degradation of CMSX-4 in terms of mechanical properties at different temperatures. They determined that it is not easy to explain this effect just with the

strain hardening mechanism. Microstructural changes as γ-channel widening, loss of interfacial coherency, coalescence of the γ′-precipitates should be taken into account [47]. Same interpretations can be made for RT-B specimens to explain the difference of elongation values.

Room temperature tensile test results are shown in Table 4.3. Although RT-A specimens have higher $R_{p0.2}$ and R_m values, they have lower elongation than RT-B specimens. According to these results, it is considered that the reason of degradation of elongation in RT-A is the existence of eutectic regions in RT-B specimens. These eutectic regions effect mechanical properties of this specimen somehow in a good way of elongation.

Table 4.3: Room temperature tensile test results.

Specimens	**$R_{p0.2}$ (MPa)**	**Rm (MPa)**	**% ε**
RT-A1	975	976	5,8
RT-A2	1060	1061	1,4
RT-B1	926	966	20,6
RT-B2	899	929	11,9

Figure 4.25 and Figure 4.26 show the stress-strain behaviour of HT-982-A and HT-982-B specimens at 982 °C, respectively and the results obtained after tests are shown in Table 4.4.

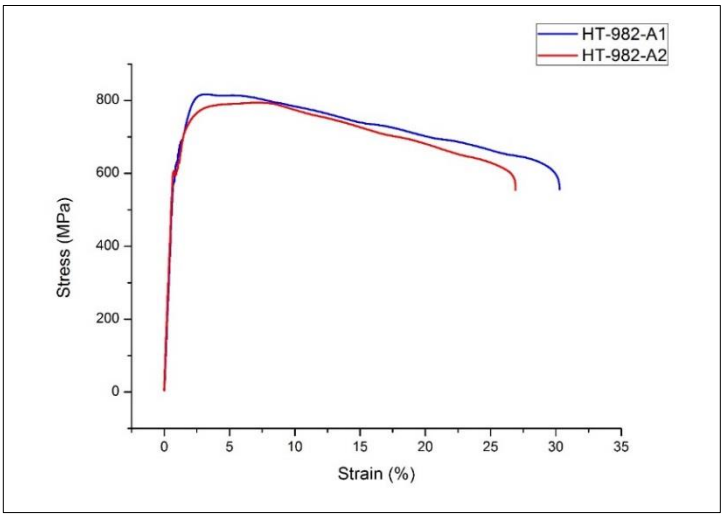

Figure 4.25: Stress-strain behaviour of standard heat treated specimens at 982 °C.

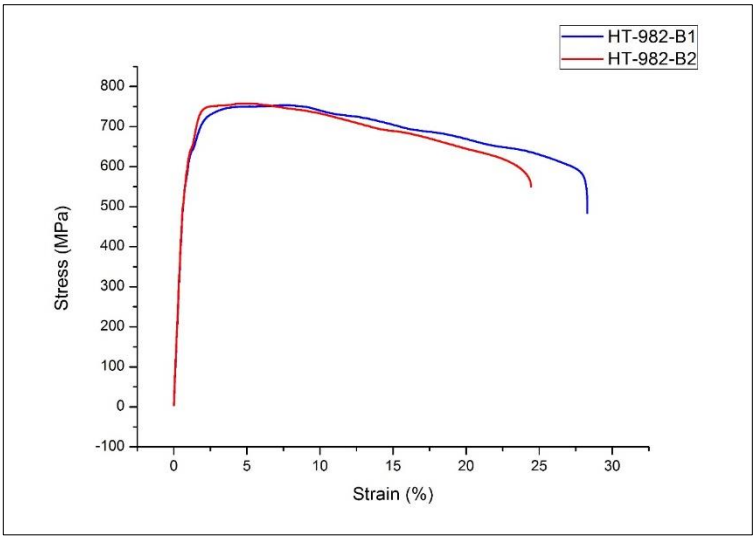

Figure 4.26: Stress-strain behaviour of modified heat treated specimens at 982 °C.

Table 4.4: High temperature tensile test results obtained at 982 °C.

HT Tensile Test results (982 °C)	**$R_{p0.2}$ (MPa)**	**Rm (MPa)**	**ε (%)**
HT-982-A1	621	817	30,03
HT-982-A2	599	794	33,68
HT-982-B1	572	753	28,67
HT-982-B2	588	758	28,74

HT-982-A and HT-982-B specimens show similar mechanical behaviour within themselves however HT-982-A specimens show higher elongation performance with the value of ~30%. The yield strength of these HT-982-A specimens have a value of 621 MPa and 599 MPa and while the tensile strengths are 817 MPa and 794 MPa, respectively. For the modified heat treated HT-982-B specimens these values are quite lower. The yield strengths are 572 MPa and 588 MPa while the tensile strengths are 753 MPa and 758 MPa, respectively. In comparison to the results obtained at room temperature tensile test, these values are lower.

Dislocations move mainly through γ matrix channels at higher temperatures. At higher temperatures, yielding is controlled by climbing process of dislocations. As mentioned before, at room temperature there is a strain-hardening effect, making the yield strength to be higher. This behaviour changes after the temperature about 800 °C[44]. At lower temperatures, thermally activated hardening is taking place, whereas

at higher temperatures thermally activated softening occurs. The yield strength is rapidly reduced and here strain softening mechanism becomes dominant factor [8, 44].

In the study made by Lapin et. al. [46], they proved that the ageing time effects inversely on the high temperature mechanical properties of CMSX-4 SX superalloys. With increasing ageing time, yield strength, ultimate tensile strength and elongation are increased slightly and then decreased. The yield strength is the most affected parameter by ageing time. It reduces most among these mechanical parameters. The ageing time of modified heat treated specimens is higher than standard heat treated specimens. As can be seen from the result shown in Table 4.4, the mechanical parameters of HT-982-B specimens are lower than HT-982-A specimens. The results are in accordance with the results obtained in that study.

The stress-strain behaviour of HT-1038-A and HT-1038-B specimens are shown in Figure 4.27 and Figure 4.28, respectively and the results are shown in Table 4.5.

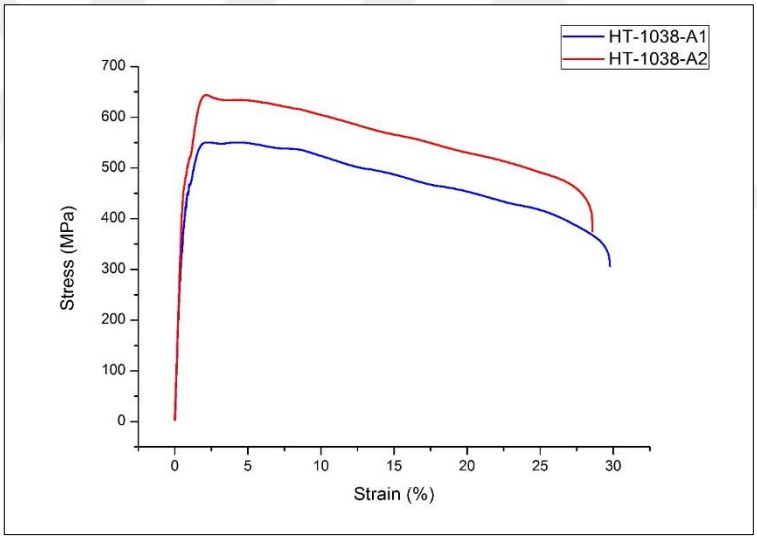

Figure 4.27: Stress-strain behaviour of standard heat treated specimens at 1038 °C.

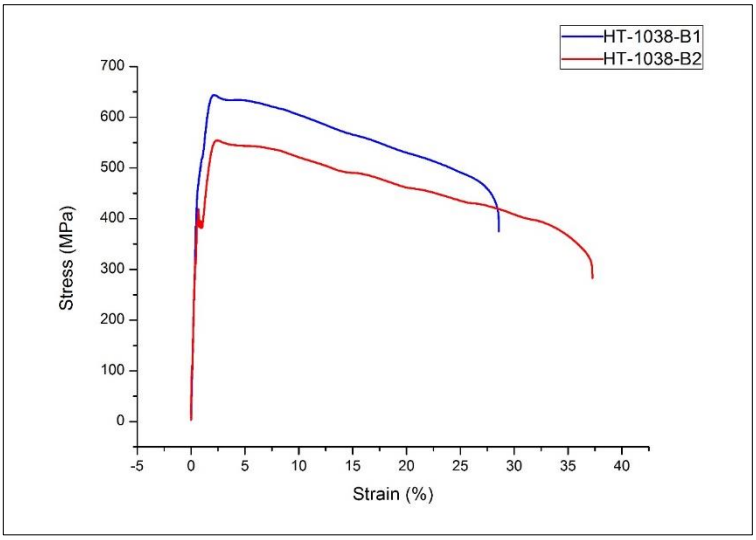

Figure 4.28: Stress-strain behaviour of modified heat treated specimens at 1038 °C.

Table 4.5: High temperature tensile test results obtained at 1038 °C.

HT Tensile Test results (1038 °C)	**$R_{p0.2}$ (MPa)**	**Rm (MPa)**	**ε (%)**
HT-1038-A1	395	550	38,9
HT-1038-A2	482	644	35,3
HT-1038-B1	449	587	34,67
HT-1038-B2	405	554	39,46

As can be expected, tensile results obtained at 1038 °C are lower than tensile tests at RT and 982 °C. With increasing temperature, the size of γ′ precipitates are increased and this results in the decreased mechanical strength. γ channels are widen, and dislocation movement effect is more dominant [34, 48]. Before the dislocation move through the γ matrix, the applied stress must be higher to overcome dislocation resistance of γ matrix [46].

After the tensile tests, new specimens were taken from HT-982 tensile test specimens in order to see changes of γ′ fraction on microstructures with the effect of high temperature during tensile test. The results are shown in Table 4.6. As can be realized that there are no changes in γ′ fraction during high temperature tensile test.

Table 4.6: γ′ fractions calculated from M specimens and HT-982 specimens.

Specimens	% γ′	Standard Deviation
M-A	70,410	2,313
HT-982-A	72,409	2,049
M-B	71,732	2,116
HT-982-B	74,428	1,798

4.4.2. Stress Rupture Test

Two specimens per heat treatment process were used for stress-rupture test. The tests were performed under 345 MPa load at 982°C. The results are shown in Table 4.7.

Table 4.7: Stress-rupture test results which performed under 345 MPa load at 982°C.

Specimen	Load	Temperature	Result
SR-A1	345 MPa	982 °C	61h 15m
SR-A2	345 MPa	982 °C	54h 8m
SR-B1	345 MPa	982 °C	28h 38m
SR-B2	345 MPa	982 °C	Failed

SR-A1 and SR-A2 specimens were ruptured in 61h 15m and 54h 8m respectively. One of the specimens of SR-B was failed while testing. The testing kits were deformed due to high temperature effect and then the test was stopped. The other specimen was ruptured in 28h 38m.

The modified heat treated specimen ruptured before the standard heat treated specimens. Various factors can affect the results. The SX superalloys are strengthened with γ′ precipitates and as a mechanical behaviour, the stress rupture properties depend on the morphology, size, volume fraction and distribution of γ′ precipitates [48]. According to the study made by Shi et. al. [48], with increasing ageing time, the rupture life of the specimens is became shorten. Shi et. al.[48] and Wilson et. al. [34] indicated that decreasing of stress rupture life depends on amount of coarsened γ′-precipitates in specimens. In SR-B specimens, there are more coarsened γ′ precipitates.

According to the study made by Zhang et al. [4], recrystallization is inversely proportional to the stress-rupture life of SX superalloys. It means that stress-rupture life of a SX superalloys is reduced with the amount of recrystallized grains. The cracks are initiated from these grains.

The micrographs were taken after stress-rupture tests and the fracture surfaces were observed with stereo microscopy and SEM. Figure 4.29, Figure 4.30 and Figure 4.31 show the fracture surfaces of SR-A1, SR-A2 and SR-B1, respectively.

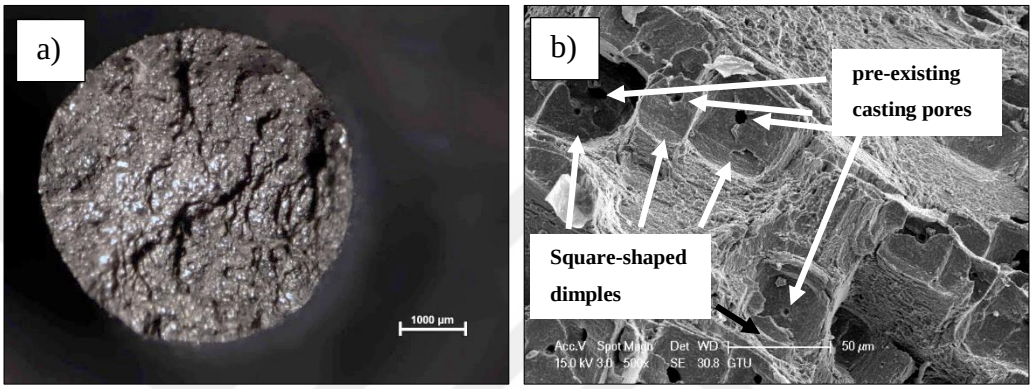

Figure 4.29: Fracture morphology of SR-A1 after stress-rupture test taken by a) stereo microscopy b) SEM

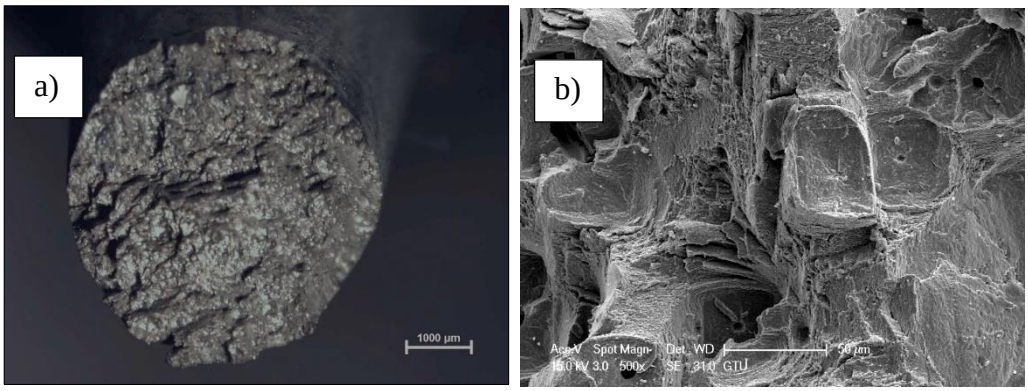

Figure 4.30: Fracture morphology of SR-A2 after stress-rupture test taken by a) stereo microscopy b) SEM

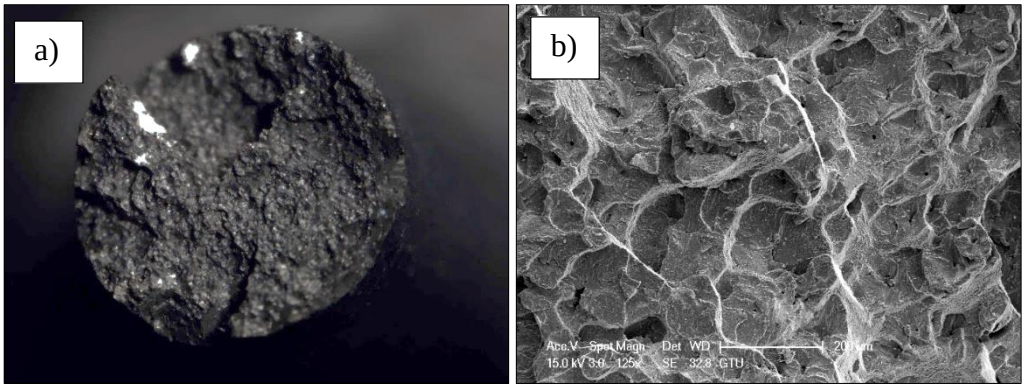

Figure 4.31: Fracture morphology of SR-B1 after stress-rupture test taken by a) stereo microscopy b) SEM

The square-shaped dimples are observed in SR-A1 and SR-A2 specimens shown in Figure 4.29 and Figure 4.30, respectively. The fracture surface is covered with lots of square-shaped dimples, and nearly every dimple has a micro-pore in the centre, which is considered as casting pore in the study made by Zhang et. al. [4]. The existence of casting pores leads the specimens to rupture, in terms of micro-cracks, before as expected. The fracture surfaces of these specimens are typical morphologies of cleavage fracture. However, the dimples are determined as a typical morphology of ductile fracture from the study made by Shi et. al. [48] but here, the fracture surface has more ductile than the SR-B specimen.

The fracture surface of SR-B1 have sharp cleavage planes and there are no square-shaped facets throughout specimen. The result of this specimen also proves this theory with lower resistance to stresses at high temperature.

In the study made by Hao et. al. [49], they have mentioned that stress−rupture life time of [001] oriented SXs is significantly longer than that of crystals with [011] or [111] orientation. With increasing temperature, the difference of rupture life time among three principal orientations is reduced, which indicates that the anisotropy of stress−rupture decreases with increasing temperature.

4.4.3. Hardness Test

The hardness test results taken from each heat-treated specimen are shown in Table 4.8.

Table 4.8: Hardness test result for as-cast and heat treated specimens.

	As-Cast Specimen	**Standard Heat treated Specimen**	**Modified Heat treated Specimen**
No.	**HV**	**HV**	**HV**
1	428	463	453
2	417	474	446
3	418	479	443
4	429	484	453
5	409	467	452
6	412	473	453
7	416	459	456
min	409	459	443
max	429	484	456
mean value	418	471	451

As can be seen from Table 4.8, Vickers hardness results of modified heat treated specimens are lower than the results of standard heat treated specimens. According to the study made by Lapin et. al. [46], Vickers hardness is inversely proportional to the ageing time of a heat treatment. The total ageing time of modified heat treatment process is 26 hours while ageing of standard heat treatment process takes 22 hours. Therefore, the results seem reasonable according to this study.

On the other hand, hardness test was performed on eutectic regions of as-cast and modified heat treated specimens in order to see if any difference occurs between two morphologies. The related results are shown in Table 4.9.

Table 4.9: Hardness test results taken from eutectic regions of as-cast and modified heat treated specimens.

	As-cast specimen	**Modified heat treated specimen**
No.	**HV**	**HV**
1	401	406
2	403	410
mean value	402	408

As can be considered from the results, there is no significant difference occurred regarding hardness between two morphologies.

5. CONCLUSIONS

5.1. Summary

CMSX-4 composition used as the main superalloy grade and two different heat treatment processes were designated based on their effects on microstructural and mechanical properties. In some level, thermodynamic approach, using the JMAT-PRO database, was used to calculate the equilibrium phase and precipitate formations. The data base was also used to select thermal processing temperatures. The objective was to generate microstructures with strength and ductility properties between that of 2nd generation single crystal alloys. The main results are as follows:

- The heat treatment of CMSX-4 superalloys provide an appealing combination of enhanced performance and production affordability for demanding, high temperature applications in advanced gas turbine engines.
- The heat treatment processes were practically a success because a range of room temperature mechanical properties was achieved, thereby a certain amount of process parameters were developed. Tough, optimization studies regarding vacuum heat treatment processes require more attention in the future considering all our experiments conducted on a box furnace.
- Hot tensile tests were satisfactory in the sense of tensile and yield stress values, tough they could not achieve elongation values compared to literature studies.
- The challenge for stress rupture resistance in this unique superalloy has not been achieved. Stress rupture strength could not exceed that of standard second generation single crystal alloys in high applied stress conditions
- Superior mechanical properties obtained by “modified heat treatment process” at room temperature mechanical testing conditions. In contrast to these result, “standard heat treatment process” showed slightly higher strength values at hot tensile and stress rupture tests.

Finally, it is considered that predicted γ and γ' formations was succeeded and it is the reason for higher room temperature mechanical properties. However, the

inhomogeneities in the microstructure and carbide formations as well as recrystallized edges challenged the high temperature mechanical properties in this study.

5.2. Contributions to the Original Knowledge

- For the first time a single crystal superalloy were cast, heat treated and characterized in Turkey.
- Two novel heat treatment process were applied, depending on the level of γ, γ' and eutectic formation and their effect on the mechanical properties were characterized.
- The effect of generated microstructures on the room and high temperature mechanical properties of CMSX-4 was studied for the first time in TÜBİTAK. Indeed, a strong effect of heat treatment on the relationship between microstructural and mechanical properties was confirmed.
- For the first time, a single crystal superalloy was conducted on hot tensile and stress rupture tests above 1000 °C in laboratory conditions of Turkey.

5.3. Recommendations of Future Work

The following observations can be considered for recommendations for future work:

- Considering the different microstructures obtained throughout these two different heat treatment studies, it can be clearly said that they have very little effect on the mechanical properties. However, it is a fact that more processing and mechanical characterizations are required for the potential of these two structures to emphasize which structure would be more ideal for SX with higher ductility concept.
- The effect of eutectic formation has been proposed as a significant mechanism in this study. However, there is no direct explanation of this no eutectic structure on the mechanical characterization (in particular high temperature mechanical properties) and this is certainly a candidate for future work (i.e., with more sample statistical analyse is required).

- A more comprehensive study is required for the γ and γ′ calculations in SX microstructure, including a new approach or modelling.
- Applying the findings to industrial conditions is necessary, particularly to properly design a solution heat treatment and ageing schedule that incorporates production line.

REFERENCES

[1] Reed R.C., (2006) "The Superalloys, Fundamentals and Applications", 1st Edition, Cambridge University Press.

[2] Martinsson Å., (2006), "Ageing Influence on Nickel-based Superalloys at Intermediate Temperatures (400–600°C)", Master's Thesis, Luleå University of Technology.

[3] Tschopp M. A., Oppedal A. L., Miller J. D., Groeber M. A., Rosenberger A. H. Solanki K. N., (2013), "Characterizing Primary Dendritic Microstructures to Quantify the Processing-Structure-Property Relationship in Single Crystal Nickel-Based Superalloys", Characterization of Minerals, Metals, and Materials, John Wiley & Sons, 299-310

[4] Zhang B., Lu X., Liu D. L., Tao C. H., (2012), "Influence of recrystallization on high-temperature stress rupture property and fracture behavior of single crystal superalloy", Materials Science and Engineering A-Structural Materials Properties Microstructure and Processing, 551, 149-153.

[5] Web 1, (2016), www.phase-trans.msm.cam.ac.uk/2003/Superalloys/superalloys.html (Erişim tarihi: 15/07/2016)

[6] Çay V., Ozan S., (2005), "Süperalaşımlar ve Uygulama Alanları", Doğu Anadolu Bölgesi Araştırmaları, 3(2), 178-188.

[7] Bahadır B., (2010), "Süperalaşımların Açık ve Kontrollü atmosferde Dökümü", Yüksek Lisans Tezi, Yıldız Teknik Üniversitesi.

[8] Fullagar K. P. L., Broomfield R. W., Hulands M., Harris K., Erickson G. L., Sikkenga S. L., (1996), "Aero engine test experience with CMSX-4(R) alloy single-crystal turbine blades", Journal of Engineering for Gas Turbines and Power-Transactions of the Asme, 118(2), 380-388.

[9] Donachie M.J., Donachie S. J., (2000), "Superalloys", 2nd Edition, ASM International, Materials Park, Ohio.

[10] Liu G., Liu L., Ai C., Ge B., Zhang J., Fu H., (2011), "Influence of withdrawal rate on the microstructure of Ni-base single-crystal superalloys containing Re and Ru", Journal of Alloys and Compounds, 509(19), 5866-5872.

[11] Kawagishi K., Yeh A. C., Yokokawa T., Kobayashi T., Koizumi Y., Harada H., (2012), "Development of an Oxidation-Resistant High-Strength Sixth-Generation Single-Crystal Superalloy TMS-238", Superalloys 2012, 189-195.

[12] Web 2, (2017), www.thenakedscientists.com/HTML/articles/article/processing-nickel-base-superalloys, (Erişim Tarihi: 01/03/2017)

[13] Bradley E. F., (1979), "Source Book on Materials for Elevated-Temperature Applications", 1st Edition, American Society for Metals.

[14] Pollock T. M., Tin S., (2006), "Nickel-based superalloys for advanced turbine engines: Chemistry, microstructure, and properties", Journal of Propulsion and Power, 22(2), 361-374.

[15] Kubiak K., Szeliga D., Sieniawski J., Onyszko A., (2015), "Chapter 11: The Unidirectional Crystallization of Metals and Alloys (Turbine Blades)", Handbook of Crystal Growth, 2nd Edition, Rzeszow University of Technology, 2B, 414-435.

[16] Durst K., Goken A., (2004), "Micromechanical characterisation of the influence of rhenium on the mechanical properties in nickel-base superalloys", Materials Science and Engineering A-Structural Materials Properties Microstructure and Processing, 387, 312-316.

[17] Zheng Y. R., Wang X. P., Dong J. X., Han Y. F., Murakami H., Harada H., (2000), "Effect of Ru addition on cast nickel base superalloy with low content of Cr and high content of W", Superalloys 2000, 305-311.

[18] Becker L., A NASA Guide to Engines. Educational Product. EG-2007-04-013-GRC.

[19] Davis J.R., (1997), "Heat Resistant Materials", 10th Edition, ASM International.

[20] Web 3, (2017), http://materialrulz.weebly.com/uploads/7/9/5/1/795167/superalloys.pdf, (Erişim Tarihi: 15/04/2017)

[21] Sims C.T., Stoloff N.S., Hagel W.C., (1987), "Superalloys II: High-Temperature Materials for Aerospace and Industrial Power", 1st Edition, John Wiley & Sons.

[22] Kazdal Zeytin H., (1998), "Silisyum Katkısının Döküm CrNiCo Süperalaşımının Özelliklerine Etkisi", Doktora Tezi, İstanbul Teknik Üniversitesi.

[23] Hagel W.C., Beattie H.J., (1959), "High Temperature Aging Structures in γ'-Hardened Austenitic Alloys", Transections of the Metallurgical Society of AIME, 215, 967-975.

[24] Wang N., Liu L., Gao S., Zhao X., Huang T., Zhang J., Fu H., (2014), "Simulation of grain selection during single crystal casting of a Ni-base superalloy", Journal of Alloys and Compounds, 586, 220-229.

[25] Gell M., Duhl D.N., Giamei A.F., (1980), "The Development of Single Crystal Superalloy Turbine Blades", Superalloys 1980, 205-214.

[26] Rzyankina, E., Pytel M., Mahomed N., Nowotnik A., (2016), "Solution Heat Treatment of Single Crystal Castings of CMSX-4 Nickel-base Superalloy", COMA'16 - International Conference on Competitive Manufacturing, Stellenbosch, 307-311.

[27] Simmonds S., (2014), "Formation and Avoidance of Surface Defects During Casting and Heat Treatment of Single-Crystal Nickel Based Superalloys" Doctoral Thesis, University of Leicester.

[28] Chapman L.A., (2004), "Application of high temperature DSC technique to nickel based superalloys", Journal of Materials Science, 39(24), 7229-7236.

[29] Wang S., (2005), "Welding and Repair of Single Crystal Ni-based Superalloys", Master's Thesis, Beijing Polytechnic University.

[30] Hegde S.R., Kearsey R.M., Beddoes J.C., (2010), "Designing homogenization-solution heat treatments for single crystal superalloys", Materials Science and Engineering A-Structural Materials Properties Microstructure and Processing, 527(21-22), 5528-5538.

[31] Szczotok A., Przeliorz R., (2012), "Phase transformations in CMSX-4 nickel-base superalloy", IOP Conference Series: Materials Science and Engineering, 35, 1.

[32] Szczotok A., (2016), "Effect of Two Different Solutionizing Heat Treatments on the Microstructure of the CMSX-4 Ni-based Superalloy", Solid State Phenomena, 246 15-18.

[33] Aslan O., (2010), "Numerical modeling of fatigue crack growth in singlecrystal nickel based superalloys", Master's Thesis, Ecole Nationale Sup´erieure des Mines de Paris.

[34] Panwisawas C., Mathur H., Gebelin J.C., Putman D., Rae C. M. F., Reed R. C., (2013), "Prediction of recrystallization in investment cast single-crystal superalloys", Acta Materialia, 61(1), 51-66.

[35] Zhang, B., Cao X. G., Liu D. L., Liu X. L., (2013), "Surface recrystallization of single crystal nickel-based superalloy" Transactions of Nonferrous Metals Society of China, 23(5), 1286-1292.

[36] Wang L., Pyczak F., Zhang J., Lou L. H., Singer R. F., (2012), "Effect of eutectics on plastic deformation and subsequent recrystallization in the single crystal nickel base superalloy CMSX-4", Materials Science and Engineering A-Structural Materials Properties Microstructure and Processing, 532, 487-492.

[37] Wang L., Pyczak F., Zhang J., Singer R. F., (2009), "On the role of eutectics during recrystallization in a single crystal nickel-base superalloy - CMSX-4", International Journal of Materials Research, 100(8), 1046-1051.

[38] Xiong J.C., Li J.R., Luo Y.S., Liu S. Z., (2012), "Surface Recrystallization and Twin Formation in a Single Crystal Superalloy", Materials Science Forum, 706-709, 2490-2495.

[39] Wilson, B.C., Hickman J.A., Fuchs G.E., (2003), "The effect of solution heat treatment on a single-crystal Ni-based superalloy" JOM, 55(3), 35-40.

[40] Karunaratne, M. S. A. Cox D.C., Carter P., Reed R.C., (2000), "Modelling of the microsegregation in CMSX-4 superalloy and its homogenisation during heat treatment", Superalloys 2000, 263-272.

[41] Kruk, A., Dubiel B., Czyrska F.A., (2014), "Examination of chemical elements partitioning between the γ and γ′ phases in CMSX-4 superalloy using EDS microanalysis and electron tomography", MATEC Web of Conferences, 14: 11004.

[42] Hemmersmeier, U., Feller K. M., (1998), "Element distribution in the macro- and microstructure of nickel base superalloy CMSX-4", Materials Science and Engineering: A, 248(1–2), 87-97.

[43] Ges, A., Fornaro O., Palacio H., (2015), "Characterization of Solution and Precipitation Temperature in CMSX-4 Superalloy" Procedia Materials Science, 8, 1127-1132.

[44] Sengupta, A., Putatunda S. K., Bartosiewicz L., Hangas J., Nailos P. J., Peputapeck M., Alberts, F. E., (1994), "Tensile behavior of a new single-crystal nickel-based superalloy (CMSX-4) at room and elevated temperatures", Journal of Materials Engineering and Performance, 3(1), 73-81.

[45] Evans W. J., Lancaster R., Steele A., Whittaker M., Jones N., (2009), "Plain and notched fatigue in nickel single crystal alloys", International Journal of Fatigue, 31(11-12), 1709-1718.

[46] Lapin, J., Gabalcová Z., Bajana O., (2009), "The effect of microstructure on mechanical properties of directionally solidified intermetallic Ti-46Al-8Nb alloy", Kovove Mater, 47(3), 159-167.

[47] Epishin A., Link T., Nazmy M., Staubli M., Klingelhöffer H., Nolze G., (2008), "Microstructural Degradation of CMSX-4: Kinetics and Effect on Mechanical Properties", Superalloys 2008, TMS, 725-731.

[48] Shi, Z., Li J., Liu S., (2012), "Effect of long term aging on microstructure and stress rupture properties of a nickel based single crystal superalloy", Progress in Natural Science: Materials International, 22(5), 426-432.

[49] Han G. M., Yang Y. H., Yu J.J., Sun X. F., (2011), "Temperature dependence of anisotropic stress–rupture properties of nickel-based single crystal superalloy SRR99", Transactions of Nonferrous Metals Society of China, 21(8), 1717-1721.

BIOGRAPHY

Gökhan GÜNAY was born in 1989 in Afyonkarahisar. He graduated from Çerkezköy Haci Fahri Zümbül Anatholian High School. He got bachelor's degree from Materials Science and Engineering in Samsun Ondokuz Mayis University in 2013. He started Master of Science degree in Gebze Technical University in 2015 and carried out the thesis working in TÜBİTAK MRC. He has been working as a research assistant in Gebze Technical University since 2015.